in the NCBI Gene Expression Omnibus (http://www.ncbi.nlm.nih.gov/geo/) and is accessible through GEO series accession number GSE25770.

Statistical analysis

Data were analysed with one-way ANOVA and Bonferroni's multiple comparison test, unless otherwise specified in the figure legends, using GraphPad Prism software version 5.00 for Windows (GraphPad Software, San Diego, CA, USA).

Author contributions

FRM conducted all *in vitro* experiments, performed the analysis of lesion volume and demyelination and wrote the paper; HK, TI, AI, AY and SN performed SCI and analysed locomotor function; TI analyzed BrdU incorporation; MMukaino analyzed the lesion scar; KS, MMatsushita and KK provided material; HK, TI, AI, MMukaino, AK, SN, HT, YM, SS and SO analyzed the data and edited the manuscript; YT, MN and HO supervised the study.

Acknowledgements

We are grateful to Gary Peltz for providing the Ro3303544 and to Shizue Ohsawa for the gift of the HRE-luc constructs. We thank Mari Fujiwara (Core Instrumentation Facility, Keio University School of Medicine) for gene expression microarray processing, Yumi Matsuzaki for advice in flow cytometry, and Tokuko Harada for mouse care. We thank all the members of Dr. Okano's laboratory for helpful discussions and support. This study was supported by the Project for the Realization of Regenerative Medicine and Support for the Core Institutes for iPS Cell Research from the Ministry of Education, Culture, Sports, Science and Technology (MEXT) in Japan, a grant-in-aid for the Global COE Program from MEXT to Keio University, a research grant from Takeda Foundation, by grants-in-aid for scientific research from MEXT (FRM, AI, and MN), fellowships from JST-SORST and the Japan Society for Promotion of Science (JSPS), as well as grants-in-aid from Keio University, JSPS, and the Naito Foundation to FRM.

Supporting information is available at EMBO Molecular Medicine online.

The authors declare that they have no conflict of interest.

References

Adachi K, Mirzadeh Z, Sakaguchi M, Yamashita T, Nikolcheva T, Gotoh Y, Peltz G, Gong L, Kawase T, Alvarez-Buylla A, *et al* (2007) Beta-catenin signaling promotes proliferation of progenitor cells in the adult mouse subventricular zone. Stem Cells 25: 2827-2836

Akiyama SK, Yamada KM (1987) Biosynthesis and acquisition of biological activity of the fibronectin receptor. J Biol Chem 262: 17536-17542

Alabed YZ, Pool M, Ong Tone S, Sutherland C, Fournier AE (2010) GSK3 beta regulates myelin-dependent axon outgrowth inhibition through CRMP4. J Neurosci 30: 5635-5643

Albiges-Rizo C, Frachet P, Block MR (1995) Down regulation of talin alters cell adhesion and the processing of the alpha 5 beta 1 integrin. J Cell Sci 108: 3317-3329

Alexander JK, Popovich PG (2009) Neuroinflammation in spinal cord injury: therapeutic targets for neuroprotection and regeneration. Prog Brain Res 175: 125-137

Araujo H, Danziger N, Cordier J, Glowinski J, Chneiweiss H (1993) Characterization of PEA-15, a major substrate for protein kinase C in astrocytes. J Biol Chem 268: 5911-5920

Azim K, Butt AM (2011) GSK3beta negatively regulates oligodendrocyte differentiation and myelination in vivo. Glia 59: 540-553

Basso DM, Fisher LC, Anderson AJ, Jakeman LB, McTigue DM, Popovich PG (2006) Basso Mouse Scale for locomotion detects differences in recovery after spinal cord injury in five common mouse strains. J Neurotrauma 23: 635-659

Beck KD, Nguyen HX, Galvan MD, Salazar DL, Woodruff TM, Anderson AJ (2010) Quantitative analysis of cellular inflammation after traumatic spinal cord injury: evidence for a multiphasic inflammatory response in the acute to chronic environment. Brain 133: 433-447

Bush TG, Puvanachandra N, Horner CH, Polito A, Ostenfeld T, Svendsen CN, Mucke L, Johnson MH, Sofroniew MV (1999) Leukocyte infiltration, neuronal degeneration, and neurite outgrowth after ablation of scar-forming, reactive astrocytes in adult transgenic mice. Neuron 23: 297-308

Chico LK, Van Eldik LJ, Watterson DM (2009) Targeting protein kinases in central nervous system disorders. Nat Rev Drug Discov 8: 892-909

Coghlan MP, Culbert AA, Cross DA, Corcoran SL, Yates JW, Pearce NJ, Rausch OL, Murphy GJ, Carter PS, Roxbee Cox L *et al* (2000) Selective small molecule inhibitors of glycogen synthase kinase-3 modulate glycogen metabolism and gene transcription. Chem Biol 7: 793-803

Cuzzocrea S, Genovese T, Mazzon E, Crisafulli C, Di Paola R, Muia C, Collin M, Esposito E, Bramanti P, Thiemermann C (2006) Glycogen synthase kinase-3 beta inhibition reduces secondary damage in experimental spinal cord trauma. J Pharmacol Exp Ther 318: 79-89

Dill J, Wang H, Zhou F, Li S (2008) Inactivation of glycogen synthase kinase 3 promotes axonal growth and recovery in the CNS. J Neurosci 28: 8914-8928

DiMilla PA, Barbee K, Lauffenburger DA (1991) Mathematical model for the effects of adhesion and mechanics on cell migration speed. Biophys J 60: 15-37

Dupin I, Camand E, Etienne-Manneville S (2009) Classical cadherins control nucleus and centrosome position and cell polarity. J Cell Biol 185: 779-786

Etienne-Manneville S, Hall A (2003) Cdc42 regulates GSK-3beta and adenomatous polyposis coli to control cell polarity. Nature 421: 753-756

Fancy SP, Baranzini SE, Zhao C, Yuk DI, Irvine KA, Kaing S, Sanai N, Franklin RJ, Rowitch DH (2009) Dysregulation of the Wnt pathway inhibits timely myelination and remyelination in the mammalian CNS. Genes Dev 23: 1571-1585

Faulkner JR, Herrmann JE, Woo MJ, Tansey KE, Doan NB, Sofroniew MV (2004) Reactive astrocytes protect tissue and preserve function after spinal cord injury. J Neurosci 24: 2143-2155

Fitch MT, Silver J (1997) Activated macrophages and the blood-brain barrier: inflammation after CNS injury leads to increases in putative inhibitory molecules. Exp Neurol 148: 587-603

Fitch MT, Doller C, Combs CK, Landreth GE, Silver J (1999) Cellular and molecular mechanisms of glial scarring and progressive cavitation: in vivo and in vitro analysis of inflammation-induced secondary injury after CNS trauma. J Neurosci 19: 8182-8198

Flugel D, Gorlach A, Michiels C, Kietzmann T (2007) Glycogen synthase kinase 3 phosphorylates hypoxia-inducible factor 1alpha and mediates its destabilization in a VHL-independent manner. Mol Cell Biol 27: 3253-3265

Forde JE, Dale TC (2007) Glycogen synthase kinase 3: a key regulator of cellular fate. Cell Mol Life Sci 64: 1930-1944

Gaudet C, Marganski WA, Kim S, Brown CT, Gunderia V, Dembo M, Wong JY (2003) Influence of type I collagen surface density on fibroblast spreading, motility, and contractility. Biophys J 85: 3329-3335

Herrmann JE, Imura T, Song B, Qi J, Ao Y, Nguyen TK, Korsak RA, Takeda K, Akira S, Sofroniew MV (2008) STAT3 is a critical regulator of astrogliosis and scar formation after spinal cord injury. J Neurosci 28: 7231-7243

Iannotti C, Zhang YP, Shields LB, Han Y, Burke DA, Xu XM, Shields CB (2006) Dural repair reduces connective tissue scar invasion and cystic cavity formation after acute spinal cord laceration injury in adult rats. J Neurotrauma 23: 853-865

Inestrosa NC, Arenas E (2010) Emerging roles of Wnts in the adult nervous system. Nat Rev Neurosci 11: 77-86

Jope RS, Yuskaitis CJ, Beurel E (2007) Glycogen synthase kinase-3 (GSK3): inflammation, diseases, and therapeutics. Neurochem Res 32: 577-595

Kapoor M, Liu S, Shi-wen X, Huh K, McCann M, Denton CP, Woodgett JR, Abraham DJ, Leask A (2008) GSK-3beta in mouse fibroblasts controls wound healing and fibrosis through an endothelin-1-dependent mechanism. J Clin Invest 118: 3279-3290

Klambt C (2009) Modes and regulation of glial migration in vertebrates and invertebrates. Nat Rev Neurosci 10: 769-779

Klapka N, Muller HW (2006) Collagen matrix in spinal cord injury. J Neurotrauma 23: 422-435

Lauffenburger DA, Horwitz AF (1996) Cell migration: a physically integrated molecular process. Cell 84: 359-369

Le QT, Denko NC, Giaccia AJ (2004) Hypoxic gene expression and metastasis. Cancer Metastasis Rev 23: 293-310

Miura K, Okada Y, Aoi T, Okada A, Takahashi K, Okita K, Nakagawa M, Koyanagi M, Tanabe K, Ohnuki M, *et al* (2009) Variation in the safety of induced pluripotent stem cell lines. Nat Biotechnol 27: 743-745

Myer DJ, Gurkoff GG, Lee SM, Hovda DA, Sofroniew MV (2006) Essential protective roles of reactive astrocytes in traumatic brain injury. Brain 129: 2761-2772

Nguyen DX, Chiang AC, Zhang XH, Kim JY, Kris MG, Ladanyi M, Gerald WL, Massague J (2009) WNT/TCF signaling through LEF1 and HOXB9 mediates lung adenocarcinoma metastasis. Cell 138: 51-62

Okada S, Nakamura M, Katoh H, Miyao T, Shimazaki T, Ishii K, Yamane J, Yoshimura A, Iwamoto Y, Toyama Y, *et al* (2006) Conditional ablation of Stat3 or Socs3 discloses a dual role for reactive astrocytes after spinal cord injury. Nat Med 12: 829-834

Okano H (2010) Neural stem cells and strategies for the regeneration of the central nervous system. Proc Jpn Acad Ser B Phys Biol Sci 86: 438-450

Palecek SP, Loftus JC, Ginsberg MH, Lauffenburger DA, Horwitz AF (1997) Integrin-ligand binding properties govern cell migration speed through cell-substratum adhesiveness. Nature 385: 537-540

Renault-Mihara F, Okada S, Shibata S, Nakamura M, Toyama Y, Okano H (2008) Spinal cord injury: emerging beneficial role of reactive astrocytes' migration. Int J Biochem Cell Biol 40: 1649-1653

Salicioni AM, Gaultier A, Brownlee C, Cheezum MK, Gonias SL (2004) Low density lipoprotein receptor-related protein-1 promotes beta1 integrin maturation and transport to the cell surface. J Biol Chem 279: 10005-10012

Scheff SW, Rabchevsky AG, Fugaccia I, Main JA, Lumpp JE Jr., (2003) Experimental modeling of spinal cord injury: characterization of a force-defined injury device. J Neurotrauma 20: 179-193

Sofroniew MV (2009) Molecular dissection of reactive astrogliosis and glial scar formation. Trends Neurosci 32: 638-647

Sun W, Hu W, Xu R, Jin J, Szulc ZM, Zhang G, Galadari SH, Obeid LM, Mao C (2009) Alkaline ceramidase 2 regulates beta1 integrin maturation and cell adhesion. FASEB J 23: 656-666

Takada Y, Ye X, Simon S (2007) The integrins. Genome Biol 8: 215

Tsuji O, Miura K, Okada Y, Fujiyoshi K, Mukaino M, Nagoshi N, Kitamura K, Kumagai G, Nishino M, Tomisato S, *et al* (2010) Therapeutic potential of appropriately evaluated safe-induced pluripotent stem cells for spinal cord injury. Proc Natl Acad Sci USA 107: 12704-12709

van Noort M, Meeldijk J, van der Zee R, Destree O, Clevers H (2002) Wnt signaling controls the phosphorylation status of beta-catenin. J Biol Chem 277: 17901-17905

Voskuhl RR, Peterson RS, Song B, Ao Y, Morales LB, Tiwari-Woodruff S, Sofroniew MV (2009) Reactive astrocytes form scar-like perivascular barriers to leukocytes during adaptive immune inflammation of the CNS. J Neurosci 29: 11511-11522

White RE, Jakeman LB (2008) Don't fence me in: harnessing the beneficial roles of astrocytes for spinal cord repair. Restor Neurol Neurosci 26: 197-214

Xia Y, Zhao T, Li J, Li L, Hu R, Hu S, Feng H, Lin J (2008) Antisense vimentin cDNA combined with chondroitinase ABC reduces glial scar and cystic cavity formation following spinal cord injury in rats. Biochem Biophys Res Commun 377: 562-566

Yoshimura T, Kawano Y, Arimura N, Kawabata S, Kikuchi A, Kaibuchi K (2005) GSK-3beta regulates phosphorylation of CRMP-2 and neuronal polarity. Cell 120: 137-149

Human Molecular Genetics, 2011, Vol. 20, No. 23 **4530–4539**
doi:10.1093/hmg/ddr394
Advance Access published on September 7, 2011

Modeling familial Alzheimer's disease with induced pluripotent stem cells

Takuya Yagi[1], Daisuke Ito[1,*], Yohei Okada[2,3], Wado Akamatsu[2], Yoshihiro Nihei[1], Takahito Yoshizaki[1], Shinya Yamanaka[4], Hideyuki Okano[2] and Norihiro Suzuki[1]

[1]Department of Neurology, [2]Departments of Physiology and [3]Kanrinmaru Project, School of Medicine, Keio University, 35 Shinanomachi, Shinjuku-ku, Tokyo 160-8582, Japan and [4]Center for iPS Cell Research and Application, Kyoto University, Kyoto 606-8507, Japan

Received June 3, 2011; Revised August 1, 2011; Accepted August 29, 2011

Alzheimer's disease (AD) is the most common form of age-related dementia, characterized by progressive memory loss and cognitive disturbance. Mutations of presenilin 1 (*PS1*) and presenilin 2 (*PS2*) are causative factors for autosomal-dominant early-onset familial AD (FAD). Induced pluripotent stem cell (iPSC) technology can be used to model human disorders and provide novel opportunities to study cellular mechanisms and establish therapeutic strategies against various diseases, including neurodegenerative diseases. Here we generate iPSCs from fibroblasts of FAD patients with mutations in *PS1* (A246E) and *PS2* (N141I), and characterize the differentiation of these cells into neurons. We find that FAD–iPSC-derived differentiated neurons have increased amyloid β42 secretion, recapitulating the molecular pathogenesis of mutant presenilins. Furthermore, secretion of amyloid β42 from these neurons sharply responds to γ-secretase inhibitors and modulators, indicating the potential for identification and validation of candidate drugs. Our findings demonstrate that the FAD-iPSC-derived neuron is a valid model of AD and provides an innovative strategy for the study of age-related neurodegenerative diseases.

INTRODUCTION

Alzheimer's disease (AD) is one of the most common neurodegenerative disorders of the elderly, characterized by progressive memory disorientation and cognitive disturbance. The pathological profile of AD is neuronal loss in the cerebral cortex accompanied by massive accumulation of two types of amyloid fibril seeding senile plaques and hyperphosphorylated tau forming paired helical filaments. The amyloid fibril is mainly composed of β-amyloid (Aβ) peptides, the 40 and 42 amino acid forms (Aβ40 and Aβ42), that are derived by proteolytic cleavages from the amyloid precursor protein (APP) by β- and γ-secretase activity (1,2). According to the amyloid cascade hypothesis, a prevailing theory of AD pathology, accumulation of Aβ, mainly Aβ42, in the brain is the initiator of AD pathogenesis, subsequently leading to the formation of neurofibrillary tangles containing hyperphosphorylated tau protein, and consequently neuronal loss (3–5).

Presenilin 1 (*PS1*) and presenilin 2 (*PS2*) genes encoding the major component of γ-secretase have been identified as the causative genes for autosomal-dominant familial Alzheimer's disease (FAD). Mutations in the *PS1* gene, located on chromosome 14, occur most frequently in FAD (6,7). Ala246Glu (A246E) in *PS1* is a well-characterized FAD mutation that shows typical phenotypes of AD with complete penetrance. Mutations in the *PS2* gene on chromosome 1 are a relatively rare cause of FAD and are variably penetrant. Asn-141 substitutions by Ile (N141I) in the *PS2* gene was the first identified causative mutation of *PS2* in affected patients from the now famous Volga German families (8,9).

Mutations in the *PS1*, *PS2* and the *APP* gene account for most of the familial early onset cases of AD either by enhancing the production of pathological Aβ or especially Aβ42, which has a greater tendency to form fibrillary amyloid deposits. These findings support β-amyloid as the common initiating factor in AD in the amyloid cascade hypothesis (10,11). Both A246E in *PS1* and N141I in *PS2* are reported to induce

*To whom correspondence should be addressed at: Department of Neurology, School of Medicine, Keio University, 35 Shinanomachi, Shinjuku-ku, Tokyo 160-8582, Japan. Tel: +81 353633788; Fax: +81 333531272; Email: d-ito@jk9.so-net.ne.jp

elevation of Aβ42 levels in human plasma, patient-derived fibroblasts, forced-expressed cells and, in mice, showing strong toxicity (10–13).

Generation of human iPSCs provides a new method for elucidating the molecular basis of human disease (14,15). An increasing number of studies have employed disease-specific human iPSCs in neurological diseases, and a few have demonstrated disease-specific phenotypes to model the neurological phenotype (16–24). Here, we report the generation of iPSC from fibroblasts of FAD with the *PS1* mutation A246E and the *PS2* mutation N141I, and differentiation of these cells into neurons. We demonstrate that patient-derived differentiated neurons increase Aβ42 secretion, recapitulating the pathological mechanism of FAD with *PS1* and *PS2* mutations. Our findings demonstrate that the FAD–iPSC-derived neuron is a valid model for studying AD, and provides important clues for the identification and validation of candidate drugs.

RESULTS

Generation of iPSC with presenilin mutations

We established two clones of iPSCs with the *PS1* mutation, A246E (PS1-2 iPSC and PS1-4 iPSC) and with the *PS2* mutation, N141I (PS2-1 iPSC and PS2-2 iPSC) by retroviral transduction of primary human fibroblasts with the five factors OCT4, SOX2, KLF4, LIN28 and NANOG. Fibroblasts were obtained from the Coriell Cell Repository (AG07768 and AG09908). The 201B7 iPSC line (14) and the sporadic Parkinson disease (PD)-derived iPSC lines (PD01-25 and 26) were reprogrammed by an original method (14) with four transcription factors (OCT4, SOX2, KLF4 and cMYC) and were used as the controls in this study. Genotyping of the established iPSC lines was confirmed by PCR–RFLP and sequencing (Fig. 1A and B). All PS1 and PS2 iPSC clones demonstrated typical characteristics of pluripotent stem cells: similar morphology to ESCs, expression of pluripotent markers including Tra-1-60, Tra-1-81, SSEA3 and SSEA4 (Fig. 1C), silencing of retroviral transgenes and reactivation of genes indicative of pluripotency (Fig. 1D). The differentiation ability of PS1 and PS2 iPSC was also confirmed *in vivo* by teratoma formation (Fig. 2), and *in vitro* by the formation of three germ layers via embryoid bodies (Supplementary Material, Fig. S1). To validate our reprogramming technique, we performed comprehensive analysis of two PS2 iPSCs. Heat map analysis showed that global gene expression profiles, including the critical genes for pluripotency, were similar between the iPSC lines established with four transcription factors (201B7 and PD01-25) and the PS2 iPSC clones established with five transcription factors (Supplementary Material, Fig. S2). In addition, there were no significant differences in the expression of AD-related molecules between PS2 iPSCs and control iPSCs (Supplementary Material, Fig. S3). Array comparative genomic hybridization (aCGH) analysis on PS2-1, PS2-2 iPSC and AG09908 fibroblasts showed that the total number of copy number aberrations were 52, 61 and 102 out of ~17 000 locations, respectively (Supplementary Material, Table S1), and no aberrations were detected in *APP*, *PS1* and *PS2* genes.

Differentiation of PS1 iPSC and PS2 iPSC into neurons

Differentiation of FAD patient-specific iPSCs towards neurons enables modeling the disease pathogenesis *in vitro*. To establish whether the presenilin mutations may affect neuronal differentiation, both PS1 and PS2 iPSC lines, as well as control iPSC lines, were induced to differentiate into neural cells (25,26), and cultured on Matrigel-coated dishes for 2 weeks to induce terminal differentiation (Fig. 3). We confirmed neuronal differentiation by the expression of neuronal markers, βIII-tubulin, and MAP-2 (Fig. 3A and B). As shown in Figure 3C, no obvious differences in the ability to generate neurons (~80% βIII-tubulin-positive cells) were observed among control, PS1 and PS2 iPSCs. This indicated that PS1 and PS2 iPSCs can generate neurons with almost the same efficiency as the control iPSCs, suggesting these presenilin mutations may have no significant effect on neuronal differentiation.

Production of Aβ secreted from iPSCs-derived neurons

To analyze the functional aspects of FAD, we investigated Aβ secretion from iPSC or iPSC-derived neurons. The Aβ secretion in the conditioned medium from control iPSC, PS1 iPSC and PS2 iPSC was very low; Aβ42 secretion especially was below the detection sensitivity. We therefore could not compare the ratio of Aβ42 to Aβ40 among iPSC lines. However, the Aβ secretion in the conditioned medium from the iPSCs-derived neurons was increased and measurable, indicating that Aβ secretion could undergo significant fluctuation during differentiation. Although the levels of Aβ42 and Aβ40 in the medium showed some clonal variation (Fig. 4A), possibly depending on the rate of cell growth and passage number, the ratio of Aβ42 to Aβ40 was significantly elevated in the PS1 and PS2 iPSCs-derived neurons, compared with the controls (Fig. 4B). Thus, PS1 and PS2 iPSCs show that living neurons derived from patients with the presenilin mutations ending at residue 42 that are linked to FAD secrete more Aβ. This result is compatible with previous evidences based on patients' plasma, fibroblasts and forced-expressed cells (10–13).

To explore recapitulation of key pathological events in AD, we investigated whether FAD-iPSC-derived differentiated neurons exhibit abnormal accumulation of tau and performed an immunoblot analysis of lysates of FAD-iPSC-derived neurons with anti-tau antibody. However, as shown in Supplementary Material, Figure S4, no abnormal tau protein accumulation or tangle formation was detected in the FAD-derived neurons, indicating that recapitulation of tauopathy is difficult to observe during the short culture period (2 weeks) in the present protocol.

Pharmacological response to γ-secretase inhibitors in PS1 iPSC- and PS2 iPSC-derived neurons

To evaluate the capacity of pharmacological drug screening in iPSC technology, we assessed whether inhibitors could affect the secretion of Aβ in PS1 and PS2 iPSCs-derived neurons. We first examined the secretion of Aβ from PS1-4 and PS2-2 iPSCs-derived neurons in the presence of Compound E, a

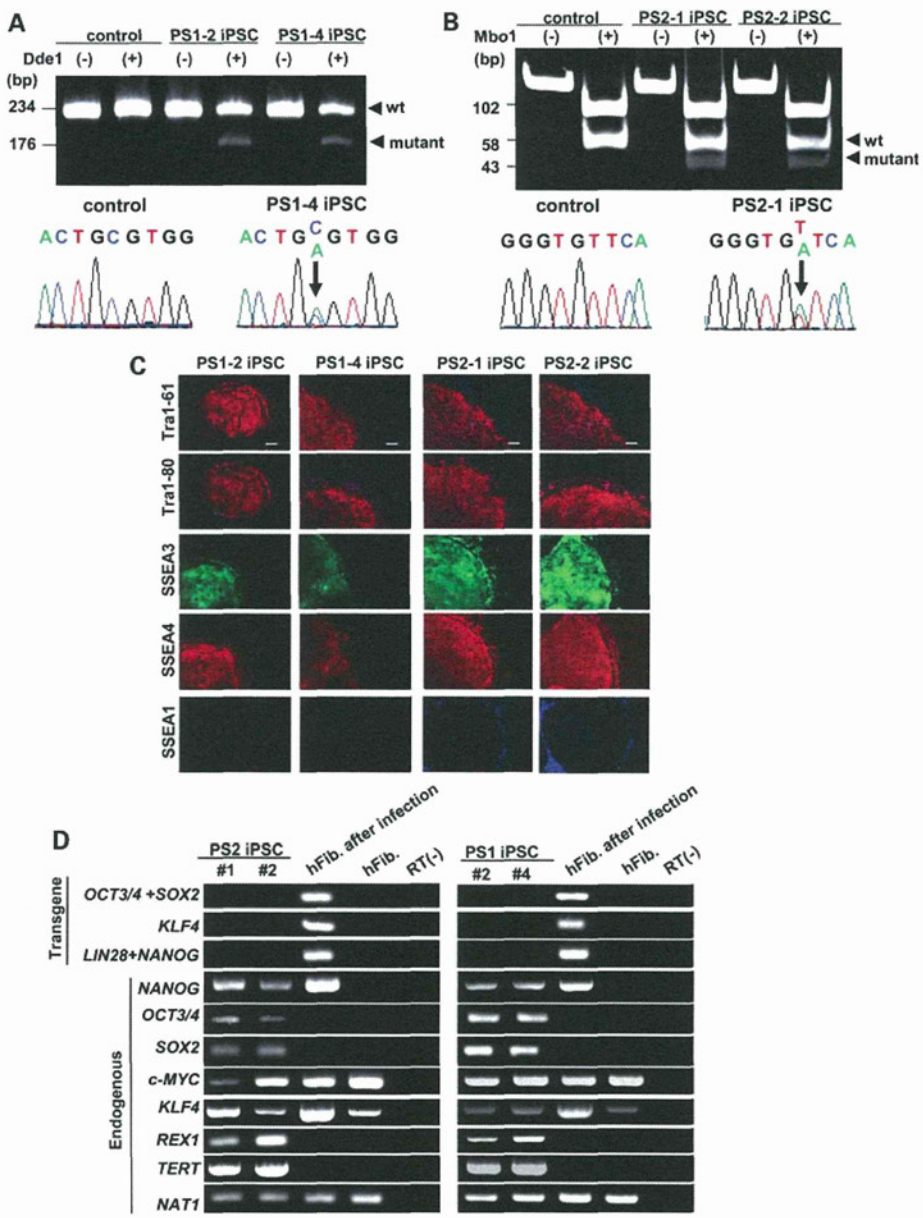

Figure 1. Generation of PS1 and PS2 iPSC from patient fibroblasts. (**A**) Genotypic analysis of PS1 iPSC by PCR–RFLP and sequencing. A246E genotyping by PCR–RFLP was performed with restriction enzyme *Dde*I. The A246E mutation results in fragments of 176 and 58 bp, whereas the control fragment has 234 bp. (**B**) Genotypic analysis of PS2 iPSC by PCR–RFLP and sequencing. N141I genotyping by PCR–RFLP was performed with restriction enzyme *Mbo*I. The N141I mutation results in fragments of 102, 58 and 43 bp, whereas the control has fragment lengths of 102 and 58 bp. (**C**) Both PS1 and PS2 iPSC lines exhibit markers of pluripotency. All iPSCs express pluripotency markers including Tra-1-60, Tra-1-81, SSEA3 and SSEA4. Nuclei were stained with 4,6-diamidino-2-phenylindole (DAPI). Bar = 200 μm. (**D**) RT–PCR analysis of the transgenes OCT3/4, SOX2, KLF4 and the endogenous hESC marker genes. Patient fibroblasts 6 days after the transduction with the retroviruses are positive for the transgenes.

potent γ-secretase inhibitor (27) (Fig. 5A and B). With the addition of 10 and 100 nM Compound E, the production of both Aβ42 and Aβ40 was suppressed in a dose-dependent manner, when compared with untreated in both of PS1-4 and PS2-2 iPSC-derived neurons. Next, we assessed the ability of Compound W, a selective Aβ42-lowering agent, to modulate γ-secretase-mediated APP cleavage (28) (Fig. 5A and B). As expected, the addition of Compound W caused a drastic decrease in the ratio of Aβ42 to Aβ40 in both neurons.

We also determined the effect of these compounds on the proteolytic processing that causes a release of an intracellular domain of Notch, another γ-secretase substrate. Western blotting using the anti-S3 cleaved Notch1-specific antibody demonstrated that productions of Notch intracellular domain

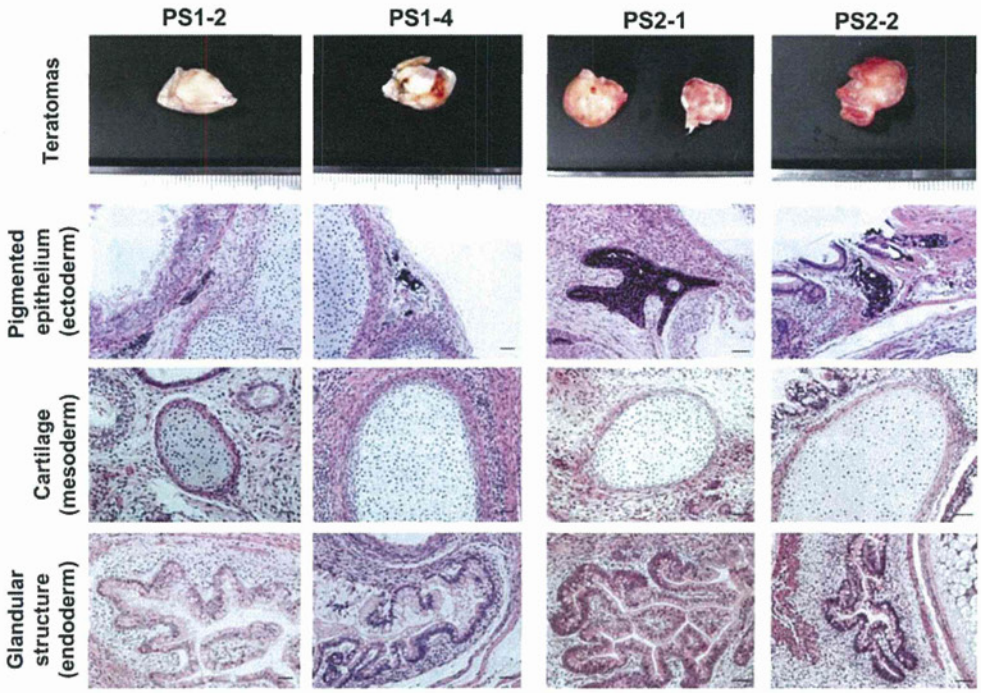

Figure 2. Teratomas derived from SCID mice injected with PS1 and PS2 iPSCs. Gross morphology, hematoxylin and eosin stained representative teratoma generated from PS 1 (PS1-2 iPSC and PS1-4 iPSC) and PS2-1 iPSC (PS2-1 iPSC and PS2-2 iPSC). Both iPSC shows tissues representing all three embryonic germ layers, including pigmented epithelium (ectoderm), cartilage (mesoderm) and glandular structure (endoderm). Bar = 50 μm.

(NICD) from both PS1-4 and PS2-2 iPSCs-derived neurons exposed to Compound E was inhibited in a dose-dependent manner. Although high dose (100 μM) of Compound W seemed to decrease NICD production in PS1-4, both neurons exposed to Compound W showed that NICD was mostly maintained (Fig. 5C). Taken together, these data indicate that both PS1 and PS2 iPSC-derived neurons respond to drug treatment in an expected manner and might be useful for drug screening in AD.

DISCUSSION

To the best of our knowledge, this study is the first to demonstrate a model of FAD using the iPSC technology. Using human neurons carrying a *PS1* mutation and a *PS2* mutation, we observed an elevation of the ratio of Aβ42 to Aβ40, a hallmark feature of FAD with presenilin mutations, in neurons derived from two clones of PS1 and PS2 iPSCs, when compared with non-AD controls (201B7, PD01-25 and 26) (Fig. 4). Although an increase in Aβ42 levels as a result of the A246E mutation in *PS1* and N141I mutation in *PS2* has been reported in patient-derived fibroblasts (11), the present study provided the first evidence of increased Aβ42 secretion by living human neurons derived from AD patients, thereby directly supporting the amyloid cascade hypothesis. To test the possibility of using the iPSC technology for drug screening, we checked the pharmacological responses to a known γ-secretase inhibitor and modulator (Fig. 5A and B). Results showed that Aβ secretion by adding agents against γ-secretase were inhibited or modulated as expected. Moreover, the Notch signaling pathway reacted with proteolytic cleavage in the presence of γ-secretase inhibitors (Fig. 5C). Recent studies have revealed that γ secretase activity is influenced in a complex manner by several cellular factors, including rafts, trafficking, expression levels of CD147, numb and gamma-secretase activating protein (1,2,29–31). We therefore propose that living human neurons from patients, i.e. FAD-iPSC-derived neurons, are very suitable material for drug development and validation of new drugs.

Previous studies on patient-specific iPSC models have mostly been limited to genetic congenital disorders (19,20,22,24,32–35). Congenital disorders may be suitable for modeling disease-specific phenotypes in the iPSC technology, because differentiated cells generated from iPSC could represent the developmental stages of disease (36). However, modeling familial PD using iPSC that carry the p.G2019S mutation in the Leucine-Rich Repeat Kinase-2 (LRRK2) gene has been reported recently (23). DA neurons derived from G2019S-iPSCs were vulnerable to exposure to stress agents, such as hydrogen peroxide, MG-132 and 6-hydroxydopamine. Now we also demonstrate the possibility of modeling the most common aging-related neurodegenerative disorder, AD, by recapitulating the key pathological mechanism (Fig. 4). Many insights into the molecular pathogenesis in neurodegenerative diseases have come from investigating post-mortem brain tissues or transgenic animals, due to the difficulty of invasive access to the living human central nervous system. With disease modeling using the iPSC technology, these new tools will make it possible to analyze living disease-specific

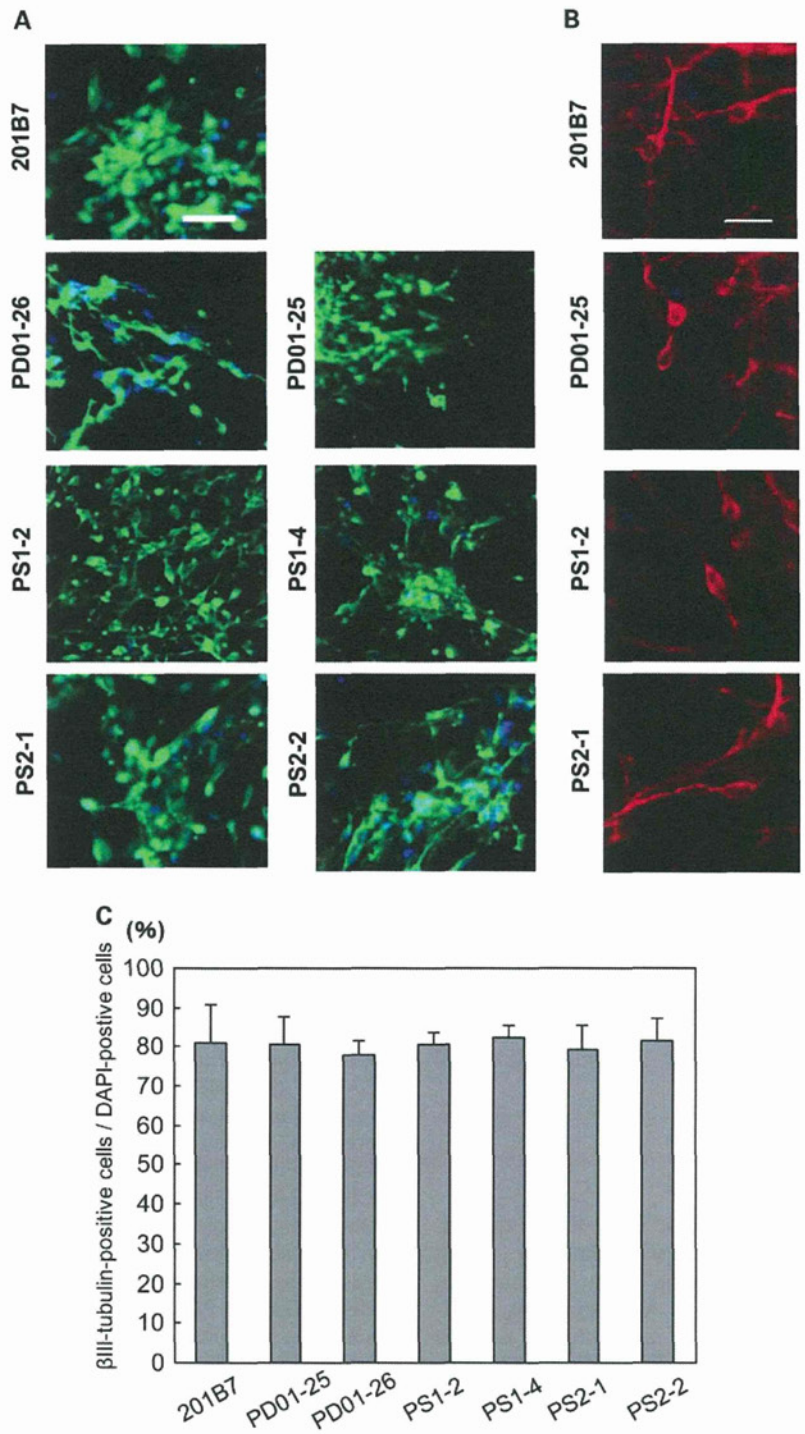

Figure 3. Differentiation of PS1 and PS2 iPSC into neurons. (**A** and **B**) Neural differentiation of control iPSC (201B7, PD01-25 and PD01-26), PS1 iPSC (PS1-2 iPSC and PS1-4 iPSC) and PS2 iPSC (PS2-1 iPSC and PS2-2 iPSC). Representative pictures of immunocytochemistry for βIII-tubulin (A) and MAP-2 (B) after neural differentiation. Bar = 40 μm (A) and 20 μm (B). (**C**) Graphs indicate the percentage of βIII-tubulin-positive cells relative to cells with DAPI-staining nuclei. Error bars indicate the SD ($n = 3$).

neurons *in vitro*. Moreover, we could graft disease-specific neurons derived from iPSCs into the brain of immunodeficient animals and we could investigate the time-dependent pathological changes *in vivo* in future studies.

FAD iPSCs could be a potential strategy for drug discovery against AD as described here; however, several limitations must be addressed in future studies. First, a high-yield of differentiated neurons from human iPSCs requires multistep

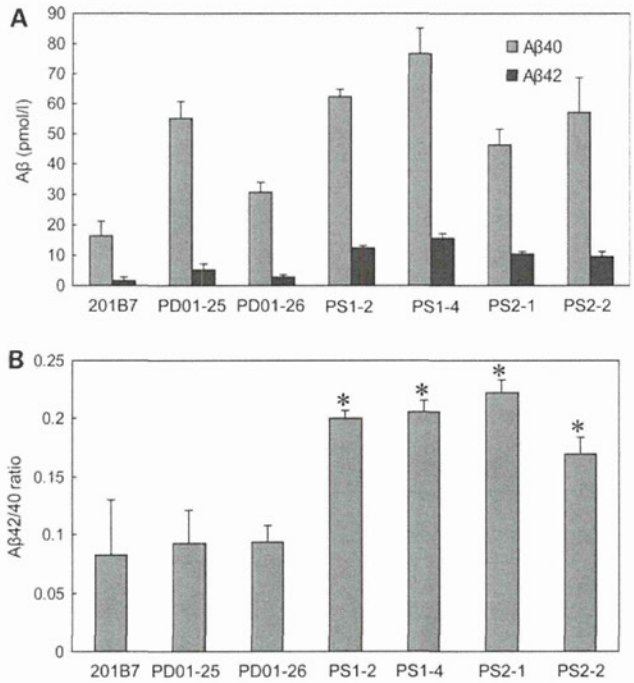

Figure 4. Characterization of Aβ secretion in PS1 and PS2 iPSC-derived neurons. (**A**) The amount of Aβ40 and Aβ42 secreted from control iPSC-derived neurons, PS1 iPSC (PS1-2 iPSC and PS1-4 iPSC) and PS2 iPSC (PS2-1 iPSC and PS2-2 iPSC)-derived neurons. (**B**) The ratio of Aβ42/Aβ40 from control iPSC-derived neurons, PS1 iPSC-derived neurons and PS2 iPSC-derived neurons. Note, the ratio of Aβ42/Aβ40 in both PS1 iPSC-derived neurons and PS2 iPSC-derived neurons was significantly higher than that of control iPSC-derived neurons. Significant differences among groups were examined by Student's *t*-test versus the ratio of 201B7 iPSC-derived neurons ($^*P < 0.05$).

procedures and prolonged culture. Furthermore, heterogeneity of differentiated neuronal cell types depending on clonal variability and culture conditions is inevitable using current differentiation methods. Clonal variation in their characters, including differentiation efficiency and tumor formation, has been a problem that needed to be solved thus far (26,37,38). Development of reliable protocols for more rapid neuronal differentiation with minimal clonal variation will be necessary, if drug discovery using iPSCs is to be fruitful. Secondly, another defining pathology in AD is an accumulation of hyperphosphorylated tau forming paired helical filaments. Growing evidence reveals that toxic Aβ directly induces tau hyperphosphorylation and accumulation, leading to neurodegeneration processes in affected neurons in AD (39,40). Pathological observations reveal that tau aggregates, but not amyloid deposits, actually correlate with dementia severity and extent of neuronal loss (41,42). Therefore, whether FAD iPSC-derived neurons exhibit accumulation of phosphorylated tau during extended culture periods should be addressed, and future studies must also focus on the biochemical dynamics of tau protein in iPSC-derived neurons treated with exogenous Aβ. Thirdly, the pathological mechanism of late-onset AD, sporadic AD and AD harboring the apoE4 allele remains unclear. Recent studies propose that impaired clearance of Aβ may cause late-onset AD through interactions with ApoE4, rather than increased Aβ production (43,44). Late-onset AD is more common and accounts for 90% of people suffering with Alzheimer's disease. To establish therapeutic strategies targeting the common form of AD, neurons derived from patient-specific iPSCs should be applied to investigations into the mechanisms underlying Aβ clearance.

Recently, a number of clinical trials of drugs targeting the pathogenesis of AD have reportedly failed in succession. Although future advances in iPSC methods are necessary for the pharmacological development and clinical application of iPSCs in neurodegeneration, we hope that our study will contribute significantly towards the identification and validation of novel candidate drugs against one of the most common and intractable diseases, AD.

MATERIALS AND METHODS

Cell culture and iPS generation

PS1 A246E fibroblasts (AG07768) and *PS2* N141I fibroblasts (AG09908) were obtained from Coriell Cell Repository. Human fibroblasts were cultured in Dulbecco's Modified Eagle's Medium (DMEM; Gibco) containing 10% fetal bovine serum, 50 U/ml penicillin, 50 mg/ml streptomycin and 1 mM L-glutamine. PS1 iPSC and PS2 iPSC were generated using the Human iPS Cell Generation Vector Set (TAKARA). G3T-hi cells were transfected with the Human iPS Cell Generation Vector set (pDON-5 OCT3/4-SOX2, pDON-5 KLF4, pDON-5 LIN28-NANOG) and pGP Vector and pE-ampho Vector with TransIT-293. Forty-eight hours after transfection, the medium (virus-containing supernatant) was collected and filtered through a 0.45 mM pore-size cellulose acetate filter. Next, the retrovirus-containing supernatant was added to RetroNectin-coated plates for centrifugation at 32°C and 2000*g* for 2 h to facilitate attachment of the virus particles onto the RetroNectin. Following this, fibroblasts were added to the plate and retrovirally transduced. Six days after transduction, fibroblasts were harvested by trypsinization and replated at 1×10^5 cells per 100 mM dish on mitomycin C-inactivated SNL cells, and the medium was changed to hiPSC medium, which consisted of DMEM/F12 medium (Invitrogen) supplemented with 20% Knock-out Serum Replacement (Invitrogen), 1 mM L-glutamine, 1 mM non-essential amino acids, 0.1 mM β-mercaptoethanol, 50 U penicillin, 50 mg/ml streptomycin (Invitrogen) and 4 ng/ml basic fibroblast growth factor (bFGF; WAKO Pure Chemicals). The hiPSC medium was changed every other day until colonies were picked. The generated iPSCs were maintained on mitomycin C-inactivated SNL cells. The hiPSC-culture medium was changed every other day, and the cells were passaged using CTK solution every 6–7 days.

Sporadic PD patient fibroblasts were generated from dermal biopsies following informed consent under protocols approved by Keio University. Two neurologists diagnosed the patient with sporadic PD, AD was excluded. Sporadic PD-derived iPSCs were generated as reported previously (14).

Reverse transcriptase-polymerase chain reaction

Total RNA samples were isolated using RNeasy (Qiagen), according to the manufacturer's instructions. The concentration

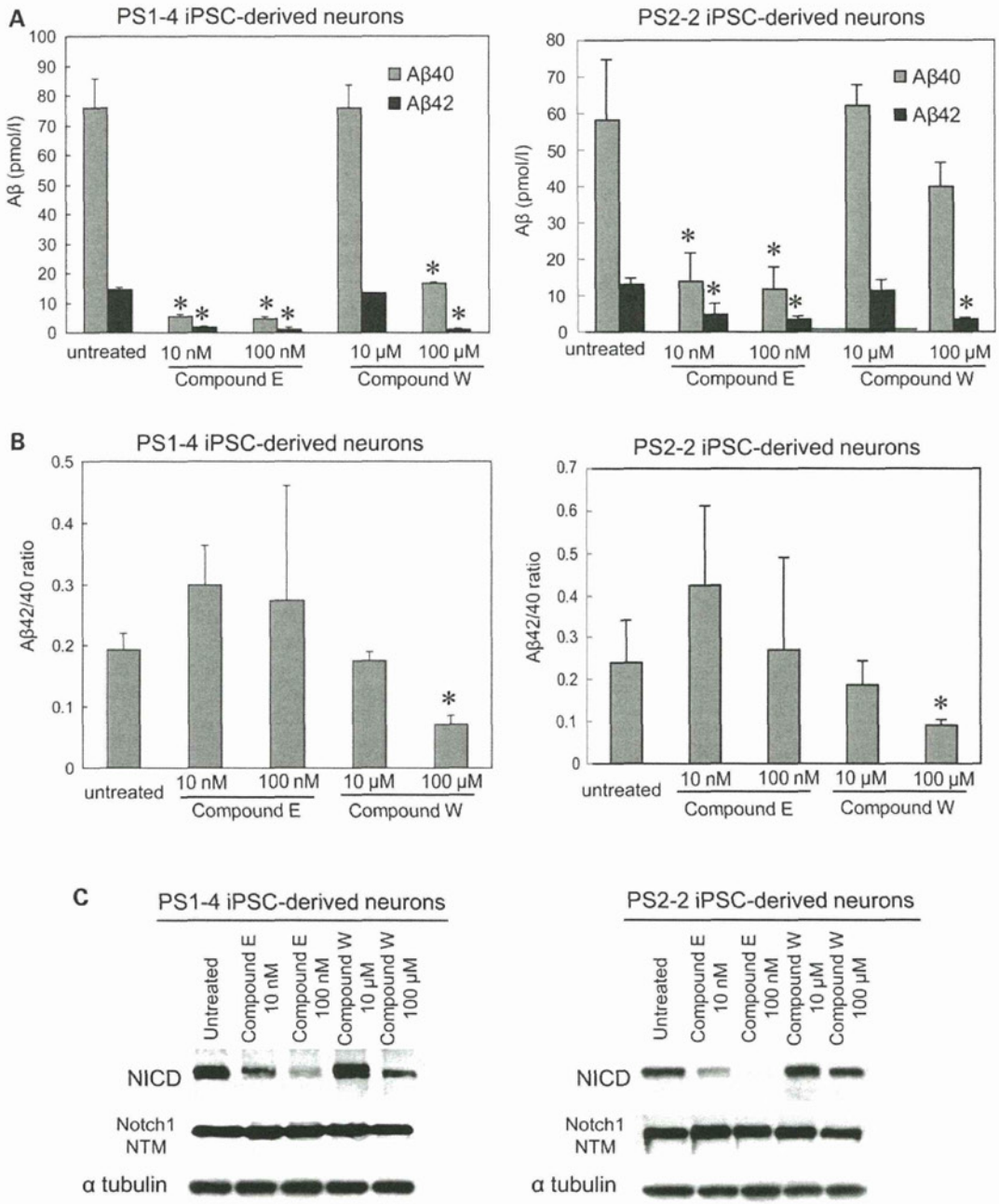

Figure 5. Pharmacological response to γ-secretase inhibitors in PS1 and PS2 iPSC-derived neurons. (**A**) The amount of Aβ40 and Aβ42 secreted from PS1-4 iPSC-derived neurons (left graph) and PS2-2 iPSC-derived neurons (right graph) treated with Compound E or W. Significant differences were examined by Student's *t*-test versus Aβ40 or Aβ42 of untreated, respectively (*$P < 0.05$). (**B**) The ratio of Aβ42/Aβ40 from PS1-4 iPSC-derived neurons (left) and PS2-2 iPSC-derived neurons (right). Significant differences were examined by Student's *t*-test versus the ratio of untreated (*$P < 0.05$). (**C**) Western blotting of S3 cleaved NICD (~110 kDa) and uncleaved Notch1 transmembrane subunit (~120 kDa) in PS1-4 iPSC-derived neurons (left) and PS2-2 iPSC-derived neurons (right) exposed to Compound E or W. α-Tubulin served as internal loading controls. Error bars in (A–D) indicate SD from three independent experiments.

and purity of the RNA was determined using the ND-1000 spectrophotometer (Nanodrop). The cDNA was synthesized using the SuperscriptIII First-Strand Synthesis System (Invitrogen). The transgene primers used in the PCR are listed in Supplementary Material, Table S2. The endogenous primers have been described previously (14).

Immunofluorescence staining of iPS and iPSC-derived differentiated neurons

Immunofluorescence staining was performed using the following primary antibodies: anti-SSEA 3 (Abcam), anti-SSEA 4 (Abcam), anti-Tra-1-60 (Millipore), anti-Tra-1-81 (Millipore),

anti-SSEA1 (Abcam), anti- MAP-2 (Chemicon) and anti-tau (HT7, Thermoscientific). 4,6-Diamidino-2-phenylindole (DAPI; Molecular Probes) was used for nuclear staining. The secondary antibodies used were: anti-rat IgG and anti-mouse IgG, and IgM conjugated with Alexa Fluor 488 or Alexa Fluor 568 (Molecular Probes).

Microarray analysis

Human genome U133 Plus 2.0 GeneChip arrays carrying 54 690 probe sets (Affymetrix) were used for microarray hybridizations to examine global gene expression. Approximately 150 ng of RNA from each sample was labeled using GeneChip 3′IVT Express (Affymetrix) according to the manufacturer's instructions. All arrays were hybridized at 45°C for 16 h and scanned using an AFX GC3000 G7 scanner. The gene expression raw data were extracted using the AFX Gene Chip Operation System. Quality control was performed on the basis of Affymetrix quality control metrics. The data were analyzed with the Gene Spring GX 11.0 (Agilent). Two normalization procedures were applied. Initially, the signal intensities with values <0.1 were assigned a value of 0.1. Then, each chip was normalized to the 50th percentile of the measurements taken from that chip. Each gene was normalized to the median of that gene in the respective controls, to enable comparisons of relative changes in gene expression levels between different conditions.

Microarray data can be found at the GEO website under accession number 'GSE28379'. (The following link has been created to allow review of record GSE28379: http://www.ncbi.nlm.nih.gov/geo/query/acc.cgi?token=zlovzkaqqwugkdg&acc=GSE28379.) The gene expression profiles of BJ fibroblasts (GSM248214) were downloaded from the NCBI Gene Expression Omnibus (GEO) database.

aCGH analysis

Genomic DNA was isolated using DNeasy (Qiagen), according to the manufacturer's instructions. DNA concentrations were measured on a Nanodrop ND-1000 spectrophotometer (Isogen). DNA quality was monitored with the Agilent 2100 Bioanalyzer (Agilent Technologies). DNA (500 ng) was labeled using the Enzo Genomic DNA Labeling kit. Hybridizations were performed on slides containing four arrays, with each array containing 622 060 *in situ* synthesized 60-mer oligonucleotides, representing 170 344 unique chromosomal locations (Agilent Technologies). Images of the arrays were acquired using a microarray scanner G2505CA (Agilent technologies) and image analysis was performed using feature extraction software version 10.7 (Agilent Technologies). The Agilent CGH-v4_107_Sep09 protocol was applied using default settings. Oligonucleotides were mapped according to the human genome build NCBI 36. The obtained data were imported into Agilent Genomic Workbench using the aberration detection method 2 (ADM-2) algorithm (10.0 threshold) for further analysis. The aCGH data have been deposited in GEO and given the series accession number GSE28450. (The following link has been created to allow review of record GSE28450: http://www.ncbi.nlm.nih.gov/geo/query/acc.cgi?token=ntsvfkqkucksgrc&acc=GSE28450.)

In vitro differentiation

Cells were harvested using CTK solutions and a cell scraper, and transferred to a Petri dish in hiPSC medium without bFGF to form embryoid bodies. After 8 days, embryoid bodies were plated onto gelatin-coated tissue culture dishes and incubated for an additional 8 days. The cells were incubated at 37°C in 5% CO_2 and the medium was replaced every other day. The cells were stained with mouse anti-α-fetoprotein IgG (R&D Systems), anti-smooth muscle actin (Sigma), anti-βIII-tubulin mouse IgG (Chemicon), together with DAPI.

Teratoma formation

hiPSCs were injected into the subcutaneous tissue of SCID mice (CREA). At 8–10 weeks post-injection, teratomas were dissected, fixed in 10% formaldehyde in PBS and embedded in paraffin.

Neural induction

Neural induction of hiPSCs cells was performed as previously described with slight modifications (Okada *et al.*, in preparation) (25,26). For terminal differentiation, induced neural cells were plated onto Matrigel-coated coverslips and cultured for 2 weeks. This was followed by the addition of Compound E, 2S-2-{[(3,5-difluorophenyl)acetyl]amino}-*N*-[(3S)-1-methyl-2-oxo-5-phenyl-2,3-dihydro-1H-1,4-benzodiazepin-3-yl]propanamide (Calbiochem) or Compound W, 3,5-Bis(4-nitrophenoxy)benzoic Acid (Tokyo Chemical Industry) for 48 h.

Quantitation of Aβ by ELISA

Conditioned media of differentiated neurons were collected after an incubation period of 48 h and subjected to β Amyloid ELISA Kits (WAKO), according to the manufacturer's instructions.

Immunoblot analysis

Cells were briefly sonicated in cold lysis buffer (50 mM Tris–HCl, pH 7.4, 150 mM NaCl, 0.5% NP-40, 0.5% sodium deoxycholate, 0.25% sodium dodecyl sulfate, 5 mM EDTA and protease inhibitor cocktail from Sigma). Total protein concentration in the supernatant was determined using a Bio-Rad protein assay kit. The proteins were then analyzed by immunoblotting as follows: protein samples were separated by reducing SDS–PAGE on a 4–20% Tris–glycine gradient gel (Invitrogen), and then transferred to a polyvinylidene difluoride membrane (Millipore). The membrane was incubated with primary antibodies and then horseradish peroxidase-conjugated secondary antibodies. Detection was performed using enhanced chemiluminescence reagents as described by the supplier (PerkinElmer Life Sciences). Primary monoclonal antibodies that were used in this study were: anti-tau (HT7, Thermoscientific), anti-NICD (Cell Signaling Technology), anti-Notch1 (D1E11) (Cell Signaling Technology) and alpha tubulin (Cell Signaling Technology).

Statistical analysis

Statistical analysis of the data was performed by Student's *t*-test using JMP 8 (SAS Institute, Inc.).

SUPPLEMENTARY MATERIAL

Supplementary Material is available at *HMG* online.

ACKNOWLEDGEMENTS

T.Y. is a research fellow of the Japan Society for the Promotion of Science. This work was supported by grants from Eisai Co. Ltd (to D.I. and N.S.) and the project for realization of regenerative medicine from the Ministry of Education, Culture, Sports, Science and Technology of Japan to H.O. We thank Mari Fujiwara (Core Instrumentation Facility, Keio University School of Medicine) for the microarray analysis and Satoko Iwasawa (Department of Preventive Medicine and Public Health, School of Medicine, Keio University) for helpful advice about statistical analysis. We also thank Dr Xu Huaxi for providing the T44 Tau pSG5 plasmid (Sanford-Burnham Medical Research Institute).

Conflict of Interest statement. None declared.

FUNDING

This work was supported by grants from Eisai Co. Ltd (to D.I. and N.S.), the Research Fellowship grant of the Japan Society for the Promotion of Science (to T.Y.), and the Project for Realization of Regenerative Medicine, and Support for Core Institutes for iPS Cell Research from the Ministry of Education, Culture, Sports, Science and Technology of Japan (to H.O.).

REFERENCES

1. Vetrivel, K.S. and Thinakaran, G. (2006) Amyloidogenic processing of beta-amyloid precursor protein in intracellular compartments. *Neurology*, **66**, S69–S73.
2. Thinakaran, G. and Koo, E.H. (2008) Amyloid precursor protein trafficking, processing, and function. *J. Biol. Chem.*, **283**, 29615–29619.
3. Hardy, J. and Selkoe, D.J. (2002) The amyloid hypothesis of Alzheimer's disease: progress and problems on the road to therapeutics. *Science*, **297**, 353–356.
4. Tanzi, R.E. and Bertram, L. (2005) Twenty years of the Alzheimer's disease amyloid hypothesis: a genetic perspective. *Cell*, **120**, 545–55.
5. Sisodia, S.S. and St George-Hyslop, P.H. (2002) gamma-Secretase, Notch, Abeta and Alzheimer's disease: where do the presenilins fit in? *Nat. Rev. Neurosci.*, **3**, 281–290.
6. Sherrington, R., Rogaev, E.I., Liang, Y., Rogaeva, E.A., Levesque, G., Ikeda, M., Chi, H., Lin, C., Li, G., Holman, K. *et al.* (1995) Cloning of a gene bearing missense mutations in early-onset familial Alzheimer's disease. *Nature*, **375**, 754–760.
7. Cruts, M., van Duijn, C.M., Backhovens, H., Van den Broeck, M., Wehnert, A., Serneels, S., Sherrington, R., Hutton, M., Hardy, J., St George-Hyslop, P.H. *et al.* (1998) Estimation of the genetic contribution of presenilin-1 and -2 mutations in a population-based study of presenile Alzheimer disease. *Hum. Mol. Genet.*, **7**, 43–51.
8. Levy-Lahad, E., Wasco, W., Poorkaj, P., Romano, D.M., Oshima, J., Pettingell, W.H., Yu, C.E., Jondro, P.D., Schmidt, S.D., Wang, K. *et al.* (1995) Candidate gene for the chromosome 1 familial Alzheimer's disease locus. *Science*, **269**, 973–977.
9. Jayadev, S., Leverenz, J.B., Steinbart, E., Stahl, J., Klunk, W., Yu, C.E. and Bird, T.D. (2010) Alzheimer's disease phenotypes and genotypes associated with mutations in presenilin 2. *Brain*, **133**, 1143–1154.
10. Borchelt, D.R., Thinakaran, G., Eckman, C.B., Lee, M.K., Davenport, F., Ratovitsky, T., Prada, C.M., Kim, G., Seekins, S., Yager, D. *et al.* (1996) Familial Alzheimer's disease-linked Presenilin 1 variants elevate Aβ1-42/1-40 ratio in vitro and in vivo. *Neuron*, **17**, 1005–1013.
11. Scheuner, D., Eckman, C., Jensen, M., Song, X., Citron, M., Suzuki, N., Bird, T.D., Hardy, J., Hutton, M., Kukull, W. *et al.* (1996) Secreted amyloid β-protein similar to that in the senile plaques of Alzheimer's disease is increased in vivo by the presenilin 1 and 2 and APP mutations linked to familial Alzheimer's disease. *Nat. Med.*, **2**, 864–870.
12. Tomita, T., Maruyama, K., Saido, T.C., Kume, H., Shinozaki, K., Tokuhiro, S., Capell, A., Walter, J., Grünberg, J., Haass, C. *et al.* (1997) The presenilin 2 mutation (N141I) linked to familial Alzheimer disease (Volga German families) increases the secretion of amyloid beta protein ending at the 42nd (or 43rd) residue. *Proc. Natl Acad. Sci. USA*, **94**, 2025–2030.
13. Oyama, F., Sawamura, N., Kobayashi, K., Morishima-Kawashima, M., Kuramochi, T., Ito, M., Tomita, T., Maruyama, K., Saido, T.C., Iwatsubo, T. *et al.* (1998) Mutant presenilin 2 transgenic mouse: effect on an age-dependent increase of amyloid beta-protein 42 in the brain. *J. Neurochem.*, **71**, 313–322.
14. Takahashi, K., Tanabe, K., Ohnuki, M., Narita, M., Ichisaka, T., Tomoda, K. and Yamanaka, S. (2007) Induction of pluripotent stem cells from adult human fibroblasts by defined factors. *Cell*, **131**, 861–872.
15. Yu, J., Vodyanik, M.A., Smuga-Otto, K., Antosiewicz-Bourget, J., Frane, J.L., Tian, S., Nie, J., Jonsdottir, G.A., Ruotti, V., Stewart, R. *et al.* (2007) Induced pluripotent stem cell lines derived from human somatic cells. *Science*, **318**, 1917–1920.
16. Dimos, J.T., Rodolfa, K.T., Niakan, K.K., Weisenthal, L.M., Mitsumoto, H., Chung, W., Croft, G.F., Saphier, G., Leibel, R., Goland, R. *et al.* (2008) Induced pluripotent stem cells generated from patients with ALS can be differentiated into motor neurons. *Science*, **321**, 1218–1221.
17. Park, I.H., Arora, N., Huo, H., Maherali, N., Ahfeldt, T., Shimamura, A., Lensch, M.W., Cowan, C., Hochedlinger, K. and Daley, G.Q. (2008) Disease-specific induced pluripotent stem cells. *Cell*, **134**, 877–886.
18. Soldner, F., Hockemeyer, D., Beard, C., Gao, Q., Bell, G.W., Cook, E.G., Hargus, G., Blak, A., Cooper, O., Mitalipova, M. *et al.* (2009) Parkinson's disease patient-derived induced pluripotent stem cells free of viral reprogramming factors. *Cell*, **136**, 964–977.
19. Ebert, A.D., Yu, J., Rose, F.F. Jr., Mattis, V.B., Lorson, C.L., Thomson, J.A. and Svendsen, C.N. (2009) Induced pluripotent stem cells from a spinal muscular atrophy patient. *Nature*, **457**, 277–280.
20. Lee, G., Papapetrou, E.P., Kim, H., Chambers, S.M., Tomishima, M.J., Fasano, C.A., Ganat, Y.M., Menon, J., Shimizu, F., Viale, A. *et al.* (2009) Modelling pathogenesis and treatment of familial dysautonomia using patient-specific iPSCs. *Nature*, **461**, 402–406.
21. Ku, S., Soragni, E., Campau, E., Thomas, E.A., Altun, G., Laurent, L.C., Loring, J.F., Napierala, M. and Gottesfeld, J.M. (2010) Friedreich's ataxia induced pluripotent stem cells model intergenerational GAA TTC triplet repeat instability. *Cell Stem Cell*, **7**, 631–637.
22. Chamberlain, S.J., Chen, P.F., Ng, K.Y., Bourgois-Rocha, F., Lemtiri-Chlieh, F., Levine, E.S. and Lalande, M. (2010) Induced pluripotent stem cell models of the genomic imprinting disorders Angelman and Prader-Willi syndromes. *Proc. Natl Acad. Sci. USA*, **107**, 17668–17673.
23. Nguyen, H.N., Byers, B., Cord, B., Shcheglovitov, A., Byrne, J., Gujar, P., Kee, K., Schüle, B., Dolmetsch, R.E., Langston, W. *et al.* (2011) LRRK2 mutant iPSC-derived DA neurons demonstrate increased susceptibility to oxidative stress. *Cell Stem Cell*, **8**, 267–280.
24. Marchetto, M.C., Carromeu, C., Acab, A., Yu, D., Yeo, G.W., Mu, Y., Chen, G., Gage, F.H. and Muotri, A.R. (2010) A model for neural development and treatment of Rett syndrome using human induced pluripotent stem cells. *Cell*, **143**, 527–539.
25. Okada, Y., Matsumoto, A., Shimazaki, T., Enoki, R., Koizumi, A., Ishii, S., Itoyama, Y., Sobue, G. and Okano, H. (2008) Spatiotemporal recapitulation of central nervous system development by murine embryonic stem cell-derived neural stem/progenitor cells. *Stem Cells*, **26**, 3086–3098.
26. Miura, K., Okada, Y., Aoi, T., Okada, A., Takahashi, K., Okita, K., Nakagawa, M., Koyanagi, M., Tanabe, K., Ohnuki, M. *et al.* (2009)

Variation in the safety of induced pluripotent stem cell lines. *Nat. Biotechnol.*, **27**, 743–745.
27. Beher, D., Wrigley, J.D., Nadin, A., Evin, G., Masters, C.L., Harrison, T., Castro, J.L. and Shearman, M.S. (2001) Pharmacological knock-down of the presenilin 1 heterodimer by a novel gamma-secretase inhibitor: implications for presenilin biology. *J. Biol. Chem.*, **276**, 45394–45402.
28. Okochi, M., Fukumori, A., Jiang, J., Itoh, N., Kimura, R., Steiner, H., Haass, C., Tagami, S. and Takeda, M. (2006) Secretion of the Notch-1 Abeta-like peptide during Notch signaling. *J. Biol. Chem.*, **281**, 7890–7898.
29. Zhou, S., Zhou, H., Walian, P.J. and Jap, B.K. (2005) CD147 is a regulatory subunit of the gamma-secretase complex in Alzheimer's disease amyloid beta-peptide production. *Proc. Natl Acad. Sci. USA*, **102**, 7499–7504.
30. He, G., Luo, W., Li, P., Remmers, C., Netzer, W.J., Hendrick, J., Bettayeb, K., Flajolet, M., Gorelick, F., Wennogle, L.P. *et al.* (2010) Gamma-secretase activating protein is a therapeutic target for Alzheimer's disease. *Nature*, **467**, 95–98.
31. Kyriazis, G.A., Wei, Z., Vandermey, M., Jo, D.G., Xin, O., Mattson, M.P. and Chan, S.L. (2008) Numb endocytic adapter proteins regulate the transport and processing of the amyloid precursor protein in an isoform-dependent manner: implications for Alzheimer disease pathogenesis. *J. Biol. Chem.*, **283**, 25492–25502.
32. Liu, G.H., Barkho, B.Z., Ruiz, S., Diep, D., Qu, J., Yang, S.L., Panopoulos, A.D., Suzuki, K., Kurian, L., Walsh, C. *et al.* (2011) Recapitulation of premature ageing with iPSCs from Hutchinson–Gilford progeria syndrome. *Nature*, **472**, 221–225.
33. Zhang, J., Lian, Q., Zhu, G., Zhou, F., Sui, L., Tan, C., Mutalif, R.A., Navasankari, R., Zhang, Y., Tse, H.F. *et al.* (2011) A human iPSC model of Hutchinson Gilford progeria reveals vascular smooth muscle and mesenchymal stem cell defects. *Cell Stem Cell*, **8**, 31–45.
34. Yazawa, M., Hsueh, B., Jia, X., Pasca, A.M., Bernstein, J.A., Hallmayer, J. and Dolmetsch, R.E. (2011) Using induced pluripotent stem cells to investigate cardiac phenotypes in Timothy syndrome. *Nature*, **471**, 230–234.
35. Carvajal-Vergara, X., Sevilla, A., D'Souza, S.L., Ang, Y.S., Schaniel, C., Lee, D.F., Yang, L., Kaplan, A.D., Adler, E.D., Rozov, R. *et al.* (2010) Patient-specific induced pluripotent stem-cell-derived models of LEOPARD syndrome. *Nature*, **465**, 808–812.
36. Mattis, V.B. and Svendsen, C.N. (2011) Induced pluripotent stem cells: a new revolution for clinical neurology? *Lancet Neurol.*, **10**, 383–394.
37. Hu, B.Y., Weick, J.P., Yu, J., Ma, L.X., Zhang, X.Q., Thomson, J.A. and Zhang, S.C. (2010) Neural differentiation of human induced pluripotent stem cells follows developmental principles but with variable potency. *Proc. Natl Acad. Sci. USA*, **107**, 4335–5340.
38. Boulting, G.L., Kiskinis, E., Croft, G.F., Amoroso, M.W., Oakley, D.H., Wainger, B.J., Williams, D.J., Kahler, D.J., Yamaki, M., Davidow, L. *et al.* (2011) A functionally characterized test set of human induced pluripotent stem cells. *Nat. Biotechnol.*, **29**, 279–286.
39. Busciglio, J., Lorenzo, A., Yeh, J. and Yankner, B.A. (1995) Beta-amyloid fibrils induce tau phosphorylation and loss of microtubule binding. *Neuron*, **14**, 879–888.
40. Jin, M., Shepardson, N., Yang, T., Chen, G., Walsh, D. and Selkoe, D.J. (2011) Soluble amyloid β-protein dimers isolated from Alzheimer cortex directly induce Tau hyperphosphorylation and neuritic degeneration. *Proc. Natl Acad. Sci. USA*, **108**, 5819–5824.
41. Bierer, L.M., Hof, P.R., Purohit, D.P., Carlin, L., Schmeidler, J., Davis, K.L. and Perl, D.P. (1995) Neocortical neurofibrillary tangles correlate with dementia severity in Alzheimer's disease. *Arch. Neurol.*, **52**, 81–88.
42. Schmitt, O., Eggers, R. and Haug, H. (1995) Quantitative investigations into the histostructural nature of the human putamen. I. Staining, cell classification and morphometry. *Ann. Anat.*, **177**, 243–250.
43. Jiang, Q., Lee, C.Y., Mandrekar, S., Wilkinson, B., Cramer, P., Zelcer, N., Mann, K., Lamb, B., Willson, T.M., Collins, J.L. *et al.* (2008) ApoE promotes the proteolytic degradation of Abeta. *Neuron*, **58**, 681–693.
44. Mawuenyega, K.G., Sigurdson, W., Ovod, V., Munsell, L., Kasten, T., Morris, J.C., Yarasheski, K.E. and Bateman, R.J. (2010) Decreased clearance of CNS beta-amyloid in Alzheimer's disease. *Science*, **330**, 1774.

Efficient and Accurate Homologous Recombination in hESCs and hiPSCs Using Helper-dependent Adenoviral Vectors

Emi Aizawa[1], Yuka Hirabayashi[1], Yuzuru Iwanaga[1], Keiichiro Suzuki[1], Kenji Sakurai[2,3], Miho Shimoji[2], Kazuhiro Aiba[2], Tamaki Wada[2], Norie Tooi[2], Eihachiro Kawase[4], Hirofumi Suemori[3], Norio Nakatsuji[5,6] and Kohnosuke Mitani[1]

[1]*Gene Therapy Division, Research Center for Genomic Medicine, Saitama Medical University, Saitama, Japan;* [2]*Stem Cell and Drug Discovery Institute, Kyoto Research Park, Kyoto, Japan;* [3]*Laboratory of Embryonic Stem Cell Research, Kyoto University, Kyoto, Japan;* [4]*Laboratory of Cell Processing, Stem Cell Research Center, Kyoto University, Kyoto, Japan;* [5]*Department of Development and Differentiation, Institute for Frontier Medical Sciences, Kyoto University, Kyoto, Japan;* [6]*Institute for Integrated Cell-Material Sciences, Kyoto University, Kyoto, Japan*

Low efficiencies of gene targeting via homologous recombination (HR) have limited basic research and applications using human embryonic stem cells (hESCs) and human induced pluripotent stem cells (hiPSCs). Here, we show highly and equally efficient gene knockout and knock-in at both transcriptionally active (*HPRT1*, *KU80*, *LIG1*, *LIG3*) and inactive (*HB9*) loci in these cells using high-capacity helper-dependent adenoviral vectors (HDAdVs). Without the necessity of introducing artificial DNA double-strand breaks, 7–81% of drug-resistant colonies were gene-targeted by accurate HR, which were not accompanied with additional ectopic integrations. Even at the motor neuron-specific *HB9* locus, the enhanced green fluorescent protein (EGFP) gene was accurately knocked in in 23–57% of drug-resistant colonies. In these clones, induced differentiation into the *HB9*-positive motor neuron correlated with EGFP expression. Furthermore, HDAdV infection had no detectable adverse effects on the undifferentiated state and pluripotency of hESCs and hiPSCs. These results suggest that HDAdV is one of the best methods for efficient and accurate gene targeting in hESCs and hiPSCs and might be especially useful for therapeutic applications.

Received 8 August 2011; accepted 11 November 2011; published online 6 December 2011. doi:10.1038/mt.2011.266

INTRODUCTION

Increasing the efficiency of gene targeting in human embryonic stem cells (hESCs) and human induced pluripotent stem cells (hiPSCs) is essential to improve both the experimental and therapeutic potential of these cells. Although gene targeting by electroporation has been routinely used in mouse embryonic stem cells (mESCs), its application in hESCs/hiPSCs has been limited.[1,2] The ratio of targeted to random chromosomal integration (the "relative" targeting efficiency) in these cell types by electroporation is generally low (0~2%).[3–7] Recently, high relative targeting efficiencies were reported in hESCs/hiPSCs by electroporating modified bacterial artificial chromosomes (BACs), encoding long homologous DNA to the target sequences.[8] Zinc-finger nucleases (ZFNs) are also used for highly efficient gene targeting at both transcriptionally active and inactive loci.[9–11] However, the accuracy of homologous recombination (HR) by these methods, which is critical for the therapeutic application of iPSCs, has not yet been proven. Viral vectors have been utilized to overcome the low DNA delivery and gene-targeting efficiencies in hESCs/hiPSCs.[9,12,13] A high-capacity helper-dependent adenoviral vector (HDAdV)[14,15] recently yielded relative targeting efficiencies of ~45% at the hypoxanthine phosphoribosyltransferase (*HPRT1*) locus in hESC lines, thus suggesting its potential as a universal gene-targeting vector in human pluripotent stem cells.[16]

The current study expanded the general applicability of HDAdVs to gene knockout and knock-in at several loci, both transcriptionally active and inactive, in hESCs as well as in hiPSCs. Efficiencies of accurate gene targeting were 7–81% at five loci without detectable effects on the undifferentiated state and pluripotency. Importantly, 75–100% of homologous recombinants were produced by accurate HR without additional vector integration at ectopic sites, suggesting high fidelity and the potential safety of HDAdV-mediated gene targeting.

RESULTS

Gene knockout of *HPRT1* locus in hiPSCs

Gene targeting at the *HPRT1* locus in hESCs was efficiently achieved using HDAdV (**Table 1**).[16] The current study first targeted the *HPRT1* locus in the male hiPSC lines, 246H1 and 246G1, using the same *HPRT1*-targeting HDAdV (**Figure 1a**).[17] HR, which knocks out the sole allele on the X chromosome, is detected by selecting the infected cells with 6-thioguanine-resistance ($6TG^R$). The cells were also subjected to negative selection with ganciclovir (GANC) to improve the relative gene-targeting efficiency because the vector also encodes the HSV*tk* gene. HDAdV infection of 246G1 cells resulted in 135 G418-resistant ($G418^R$) colonies, 79 of which were $G418^R$-GANC-resistant ($GANC^R$). Of those $G418^R$-$GANC^R$

Correspondence: *Kohnosuke Mitani, Gene Therapy Division, Research Center for Genomic Medicine, Saitama Medical University, Hidaka, Saitama 350-1241, Japan. E-mail: mitani@saitama-med.ac.jp*

Table 1 Summary of gene-targeting efficiencies in human ESCs and iPSCs

Cell line	Locus	Delivery method	Treated cells	G418^R colonies	G418^R-GANC^R colonies	Targeted integration[a]	Accurate gene targeting			
							Confirmed/ analyzed[b]	Per cell[c]	Per G418Rd	Per G418^R GANCRd
KhES-1[e]		HDAdV	5.1×10^6	136	31	14 (10%)	14/14 (100%)	2.7×10^{-6}	10%	45%
KhES-3[e]		HDAdV	1.9×10^6	14	6	2 (14%)	2/2 (100%)	1.1×10^{-6}	14%	33%
KhES-1[e]	*HPRT1*	EP	1.1×10^8	172	98	1 (1%)	N.D.	9.1×10^{-9}	0.6%	1%
246G1		HDAdV	2.5×10^7	135	79	16 (12%)	5/5 (100%)	6.4×10^{-7}	12%	20%
246H1		HDAdV	5.1×10^6	39	14	1 (3%)	1/1 (100%)	2.0×10^{-7}	3%	7%
246H1		EP	2.1×10^8	126	93	0 (0%)		0		
KhES-3	*HB9*	HDAdV	5.0×10^6	172	21	12 (7%)	12/12 (100%)	2.4×10^{-6}	7%	57%
246H1		HDAdV	1.7×10^6	280	61	14 (5%)	3/3 (100%)	8.2×10^{-6}	5%	23%
246H1	*LIG3*	HDAdV	4.4×10^6	164	73	41 (25%)	3/4 (75%)	7.0×10^{-6}	19%	42%
246H1	*LIG1*	HDAdV	4.4×10^6	93	28	12 (13%)	4/5 (80%)	2.2×10^{-6}	10%	34%
246H1	*KU80*	HDAdV	2.2×10^6	227	153	124 (55%)	3/3 (100%)	5.6×10^{-5}	55%	81%
Summary of HDAdV-mediated gene targeting										
4	5	9 experiments		1,260	466	3–55%	47/49 (75–100%)	2.0×10^{-7} to 5.6×10^{-5}	3–55%	7–81%

EP, electroporation; ESCs, embryonic stem cells; GANC, ganciclovir; HDAdV, helper-dependent adenoviral vector; HPRT1, hypoxanthine phosphoribosyltransferase; iPSCs, induced pluripotent stem cells; N.D., not determined.
[a]G418^R-GANC^R colonies with the vector integrated at the target locus was determined by PCR analyses. [b]Accuracy of gene targeting was determined by Southern analyses. [c]The absolute (per cell) targeting efficiencies were calculated as (the number of targeted integration) × (% confirmed by Southern analyses) / (the number of treated cells). [d]The relative (per chromosomal integration) targeting efficiencies were calculated as (the number of targeted integration) × (% confirmed by Southern analyses) / (the number of drug-resistant colonies). [e]These data were previously published.[16]

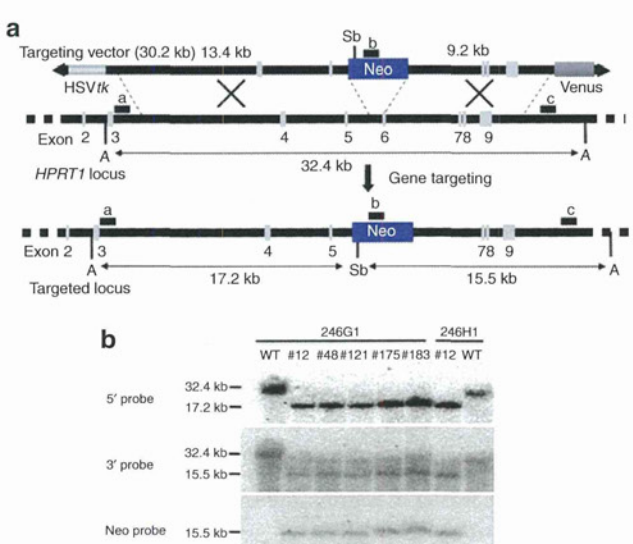

Figure 1 Gene targeting at *HPRT1*. (**a**) Schematic illustration of *HPRT1* knockout with HDAdV. The probes for Southern analyses are shown as black bars. a, 5′ probe; b, neo probe; c, 3′ probe. HSV*tk*, the herpes simplex virus thymidine kinase gene cassette; Neo, the neomycin-resistant gene cassette; Venus, an expression cassette for the Venus (F46L mutant yellow fluorescent protein gene ref. 41); A, *Ahd*I sites; Sb, *Sbf*I sites. (**b**) Southern analyses of wild type (WT) and the *HPRT1*-knockout human induced pluripotent stem clones. Genomic DNA was digested with *Ahd*I and *Sbf*I. HDAdV, helper-dependent adenoviral vector.

colonies, 16 were also 6TG^R. The resultant gene-targeting efficiency (G418^R-GANC^R-6TG^R colonies)/(G418^R-GANC^R colonies) was 20% with positive-negative selection (**Table 1**). A similar efficiency of 7% was observed in the 246H1 cell line (**Table 1**). The linearized *HPRT1*-targeting HDAdV plasmid was electroporated into the 246H1 cells as a control, resulting in no HR out of 126 G418^R clones. Southern hybridization (**Figure 1b**) demonstrated that those 6TG^R clones had been targeted accurately at the *HPRT1* locus via HR, without ectopic vector integration (**Supplementary Figure S1a**). These results indicate that HDAdV-mediated gene targeting is equally efficient in both hESCs and hiPSCs.

Heterozygous knockout of *KU80*, *LIG1*, and *LIG3* genes in hiPSCs

Next, to examine the applicability of HDAdV-mediated gene targeting at other housekeeping loci, the Lupus Ku autoantigen protein p80 (*KU80*) locus of the nonhomologous end-joining (NHEJ) pathway, and the DNA Ligase I (*LIG1*) and DNA Ligase III (*LIG3*) loci of the potential backup pathway of NHEJ were targeted. NHEJ is a major pathway involved in DNA double-strand break (DSB) repair. *KU70* and *KU80* are the key factors in NHEJ, and the heterozygous mutant cells or RNAi-induced knockdown of Ku resulted in elevated gene-targeting frequencies via HR in the HCT116 and NALM-6 human somatic cell lines.[18,19] The 246H1 cells were infected with gene-targeting HDAdVs that were designed to delete exons 3–4 of *KU80*, exons 3–4 of *LIG1*, and exons 5–7 of *LIG3* (**Figures 2a** and **3a,b**). Detailed Southern analyses of G418^R and GANC^R clones revealed relative gene-targeting efficiencies of 81% at *KU80*, 34% at *LIG1*, and 42% at *LIG3* (**Figures 2b** and **3c**, **Supplementary Figure S1b–d**, **Table 1**). Importantly, in contrast to ZFN-mediated gene targeting, no ectopic vector integration was observed in any of these targeted clones (**Supplementary Figure S1b–d**). In these heterozygous hiPS clones, the inserted neomycin-resistant gene (*neo*) was flanked by the mutant *lox*P sites (*lox*71 and *lox*66). After transfection of pCAGGS-Cre, which encodes the

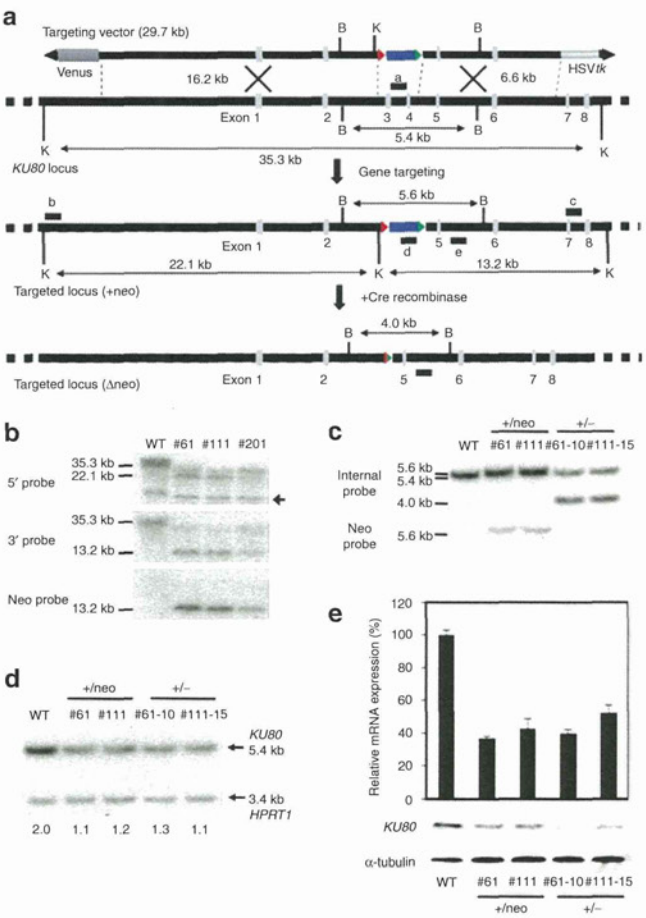

Figure 2 Gene targeting at *KU80*. (**a**) Schematic illustration of *KU80* heterozygous knockout with HDAdV. The probes for Southern analyses are shown as black bars; a, neo probe; b, 5′ probe; c, 3′ probe; d, deleted-region probe; e, internal probe. HSV*tk*, the herpes simplex virus thymidine kinase gene cassette; Blue box, the neomycin-resistant gene cassette; Venus, the Venus gene cassette; Triangle, *lox*P site; B, *Bgl*II sites; K, *Kpn*I sites. (**b**) Southern analyses of WT (246H1) and heterozygous knockout clones (#61 and #111). #201 is an inaccurate recombinant. Genomic DNA was digested with *Kpn*I. An arrow indicates a nonspecific band. (**c**) Southern hybridization analyses of the *KU80* heterozygous knockout clones obtained from 246H1, and the clones from which the PGKneo cassette was removed by transient Cre expression. The genomic DNA was digested with *Bg* II and hybridized to the ^{32}P-labeled internal probe or neo probe. WT, wild-type parental cells. (**d**) Quantitative Southern hybridization. Genomic DNA was digested with *Bgl*II and hybridized with probe "d." A DNA fragment from intron 3 of *HPRT1* locus was used as a control probe. The copy number of wild-type *KU80* allele determined by a densitometric analysis is indicated. (**e**) Reduction of *KU80* gene expression in the heterozygous mutants. The upper panel indicates the mRNA level determined by quantitative RT-PCR. The average of three independent experiments is shown with the standard deviation. The lower panel indicates the protein level determined by Western blot. An anti-α-tubulin antibody was used as a loading control. HDAdV, helper-dependent adenoviral vector. RT-PCR, reverse transcription-PCR.

CAG promoter-driven Cre gene, and recloning of the cells, *neo* was removed in ~25% of the cells (**Figures 2c** and **3d**, **Supplementary Figure S1b–d**, **Supplementary Table S1**). Two independent clones from *LIG1*, *LIG3*, and *KU80* heterozygous mutant iPSCs were subjected to further analyses. The reduction in the copy number of wild-type (WT) allele and of gene expression levels in these heterozygous hiPS clones were confirmed by quantitative genomic Southern analyses, quantitative reverse transcription-PCR (RT-PCR), and western blotting (**Figures 2d,e** and **3e,f**). These results therefore indicate that highly efficient gene targeting can be achieved at various housekeeping loci using HDAdVs.

Gene knock-in of *HB9* locus in hESCs and hiPSCs

Next, to examine the efficiency of HDAdV-mediated gene targeting at transcriptionally inactive loci, reporter hESC and hiPSC lines were established, in which the enhanced green fluorescent protein (EGFP) gene was knocked into the *HB9* locus by HR. *HB9* is expressed selectively in motor neurons in the developing vertebrate central nervous system and also in pancreatic cells, but not in ES cells.[20–22] A human *HB9*-targeting HDAdV was constructed with homology arms of 12.1 kb and 2.0 kb on each side (**Figure 4a**). The infected hESC line, KhES-3, had 21 GANC^R colonies out of 172 G418^R (**Table 1**). Southern hybridization demonstrated that 12 of these 21 colonies (57%) had been accurately targeted at the locus, without ectopic vector integration (**Figure 4b**, **Supplementary Figure S1e,f**). In addition to hESCs, the *HB9* locus was also targeted in the hiPSC line, 246H1, at similar efficiencies (**Table 1**, **Figure 4b**). A karyotype analysis was performed for the knock-in hESC clones G1 and 47, and no abnormality was observed by G-banding (**Supplementary Figure S2**). We also performed a similar analysis for the *HPRT1*-knockout hESC clone, which we reported previously, and found no abnormalities (**Supplementary Figure S2**), *HB9*-targeted hESCs and hiPSCs maintained an undifferentiated state (**Figure 5a**) and pluripotency (**Figure 5b,c**), as we have previously reported for the *HPRT1*-knockout hESC clones.[16] These results indicate that HDAdV-mediated gene targeting is equally efficient regardless of the transcriptional activities of target loci.

The *HB9*-EGFP knock-in hiPSC line was induced to differentiate into motor neurons to validate differentiation-specific expression of the knocked-in EGFP gene in these reporter cell lines. The *neo* cassette, which is sandwiched by *lox*P sites, was excised from the knock-in iPSC clone by transient expression of Cre recombinase (**Figure 4a**) because the presence of drug-resistant gene may interfere with regulated expression of the reporter gene. After transfection with the pCAGGS-Cre plasmid, followed by analyses of G418 sensitivity and PCR, it was confirmed that the drug-resistant cassette was excised from the *HB9* locus in ~50% of the cells (**Supplementary Table S1**).

The immunofluorescence analysis of *HB9*-EGFP knock-in hiPSC and hESC lines revealed a correlation between EGFP and *HB9* expression (**Figure 4c**, **Supplementary Figure S3**). All of the EGFP-positive cells were *HB9*-positive by immunostaining, suggesting the EGFP gene was precisely knocked into the target chromosomal site by HDAdV-mediated gene targeting. Together, these results demonstrated that HDAdVs are a powerful tool for efficient and accurate gene knockout and knock-in in hESCs and hiPSCs.

DISCUSSION

Various attempts have been made to improve gene-targeting efficiencies in hESCs/hiPSCs. Four methods have been reported,

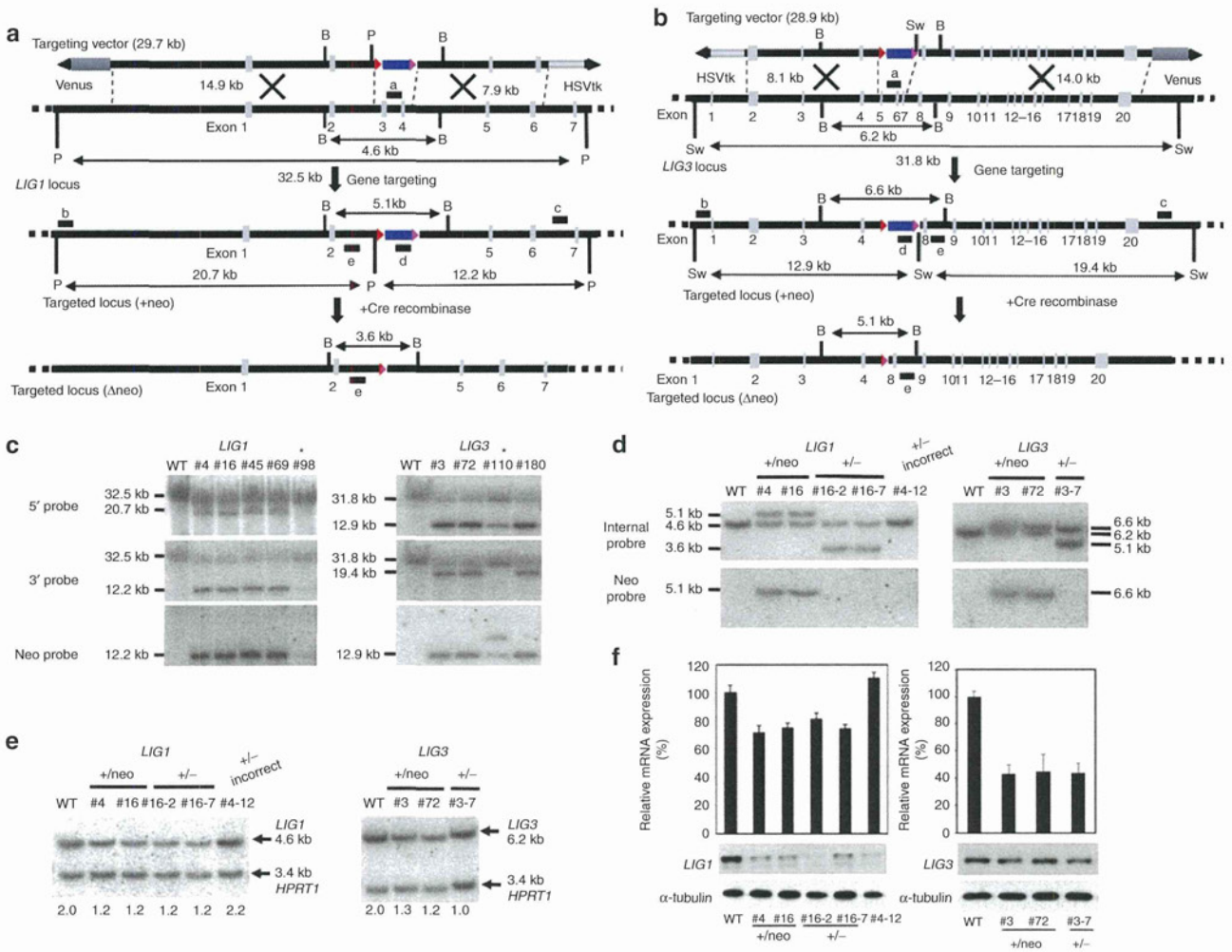

Figure 3 Generation of *LIG1* and *LIG3* heterozygous mutants in human induced pluripotent stem cells. **(a)** Schematic illustration of the *LIG1* heterozygous knockout with HDAdV. The probes for Southern hybridization analyses are shown as black bars; a, neo probe; b, 5′ probe; c, 3′ probe; d, deleted-region probe; e, internal probe. HSV*tk*, the herpes simplex virus thymidine kinase gene cassette; Blue box, the neomycin-resistant gene cassette; Venus, the Venus gene cassette; Triangle, *lox*P site; B, *Bgl*II; P, *Pac*I. **(b)** Schematic illustration of the *LIG3* heterozygous knockout in human induced pluripotent stem cells. The probes for Southern hybridization analyses are shown as black bars; a, neo probe; b, 5′ probe; c, 3′ probe; d, deleted-region probe. HSV*tk*, the herpes simplex virus thymidine kinase gene cassette; Neo, the neomycin-resistant gene cassette; Venus, the Venus gene cassette; Red triangle, *lox*P site; B, *Bgl*II; Sw, *Swa*I. **(c)** Southern hybridization analyses of WT, *LIG1*, and *LIG3* heterozygous knockout clones (*LIG1*: #4, #16, #45, and #69; *LIG3*: #3, #72, and #180). Genomic DNA was digested with *Pac*I or *Swa*I. Asterisks indicate inaccurate homologous recombinants. **(d)** Southern hybridization analyses of the *LIG1* and *LIG3* heterozygous knockout clones obtained from 246H1 cells and clones in which the PGKEM7neo cassette was removed by transient expression of Cre recombinase to confirm the insertion and removal of the PGKneo cassette. The genomic DNA was digested with *Bgl*II and hybridized with the ^{32}P-labeled internal probe or neo probe. #4-12 is an inaccurate recombinant. WT, wild-type parental cells. **(e)** Quantitative Southern hybridization. Genomic DNA was digested with *Bgl*II and hybridized with probe "d." A DNA fragment from intron 3 of the *HPRT1* locus was used as a control probe to normalize the amount of loaded DNA. The copy number of wild-type *LIG1* or *LIG3* allele determined by a densitometric analysis is indicated. **(f)** Reduction of *LIG1* (left panel) or *LIG3* (right panel) gene expression at mRNA and protein levels in the heterozygous *LIG1* or *LIG3* mutants. The upper panel indicates the mRNA level determined by quantitative RT-PCR. The average of three independent experiments is shown with the standard deviation. The lower panel indicates the protein level determined by Western blotting. An anti-α-tubulin antibody was used as a loading control. HDAdV, helper-dependent adenoviral vector. RT-PCR, reverse transcription-PCR.

which routinely achieve high relative targeting efficiencies in hESCs/hiPSCs. The first method is electroporation of BAC-based gene-targeting constructs with large homologies.[8] The relative gene-targeting efficiencies were ~33% at three housekeeping loci. However, gene targeting at transcriptionally inactive loci has not yet been reported. The second method utilizes the ZFNs, which are fusion proteins of sequence-specific zinc-finger DNA-binding domains and a nonspecific *Fok*I nuclease domain.[23,24] Carefully designed ZFNs introduce a chromosomal DSB at the target site, which greatly enhances the frequency of HR repair near the DSB.[25] Several groups have validated the use of ZFNs to target chromosomal loci in hESCs/hiPSCs with high relative targeting efficiencies of 6–100%.[9–11] However, frequent DSBs at off-target sites, accompanied by inaccurate NHEJ repair and ectopic integration of gene-targeting cassettes, have been observed after ZFN treatment in hESCs/hiPSCs and in other cell types.[10,11,26–28] The third method utilizes adeno-associated virus (AAV) vectors, with the relative targeting efficiencies of 1–30%.[12,13,29] The gene-targeting

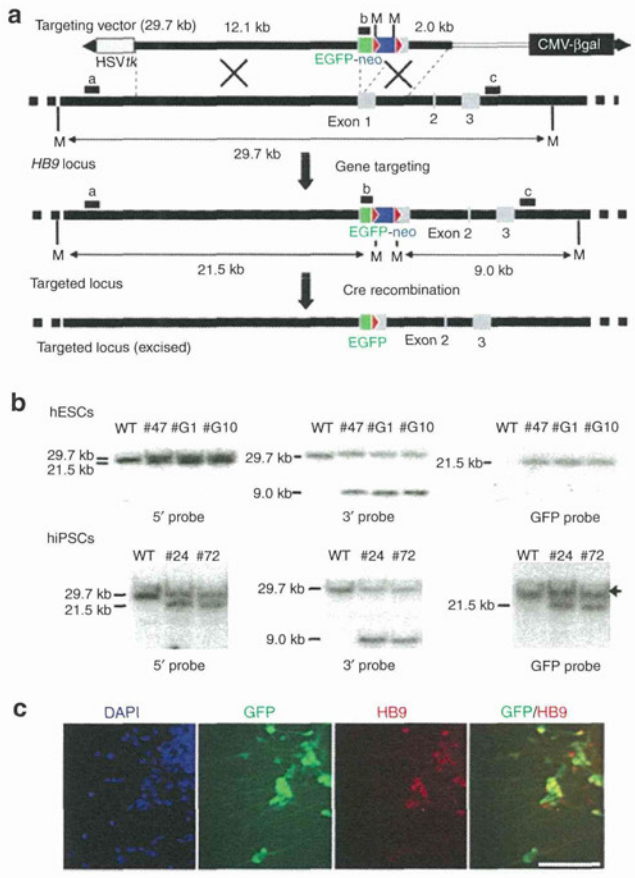

Figure 4 Generation of *HB9*-EGFP knock-in reporter cell lines from hESCs and hiPSCs. (**a**) Schematic illustration of *HB9*-EGFP knock-in with HDAdV. The probes for Southern analyses are shown as black bars. a, 5′ probe; b, EGFP probe; c, 3′ probe. Green box, the EGFP gene. Blue box, the neomycin-resistant gene. Red triangle, *lox*P site. White bar, stuffer DNA for adjusting the vector size. CMV-βgal, the βgal expression cassette; M, *Mfe*I sites. (**b**) Southern analyses of wild-type parental and the *HB9*-EGFP knock-in clones (hESC: #47, #G1, and #G10; hiPSC: #24 and #72). Genomic DNA was digested with *Mfe*I. An arrow indicates a signal from the "endogenous" GFP gene, which was encoded by a retroviral vector used for induction of iPSCs. (**c**) Immunofluorescence analysis of motor neurons differentiated from the *HB9*-EGFP knock-in hiPSC clone (#24). Bar, 100 µm. EGFP, enhanced green fluorescent protein; HDAdV, helper-dependent adenoviral vector; hESCs, human embryonic stem cells; hiPSCs, human induced pluripotent stem cells.

efficiency can also be evaluated by the efficiency per treated cell (we call this the "absolute" targeting efficiency). The absolute targeting efficiency by the BAC-based method is generally low, at 5×10^{-8} to 5×10^{-7} per cell. In the case of the ZFN-mediated method, the absolute efficiencies were ~7×10^{-5} per cell.[11] Homozygous mutant hESCs/hiPSCs could also be obtained by a one-step process.[10] The absolute efficiencies by the AAV-based method range from 1.9×10^{-7} to 2.4×10^{-4} per cell.[29] While both the relative and absolute targeting efficiencies are high, the AAV vectors have limitations for certain applications, such as the small cloning capacity of ~4.7 kb and the relative inefficiency of targeting silent loci.[29] In addition to these methods, oligonucleotide-mediated gene modification might be another efficient method, which achieved the absolute efficiencies of -2×10^{-4} per cell in mouse ESCs,[30] although its application to hESCs/hiPSCs has not been reported.

The fourth method involves delivering gene-targeting cassettes using HDAdV. In this study, we demonstrated the versatility of HDAdV in a variety of gene knockouts (*HPRT1*, *LIG1*, *LIG3*, and *KU80*) and knock-ins (*HB9*) in multiple hESC and hiPSC lines. *KU80*, *LIG1*, and *LIG3* heterozygous mutant hiPSCs will be useful for analyzing the biological functions of the genes in human pluripotent stem cells and, potentially, to achieve improved efficiencies of gene targeting in these mutant hiPSCs. A knock-in of a fluorescent marker gene into the hapatocyte-specific *ALB* locus also showed similar targeting efficiencies in hESCs/hiPSCs (manuscript in preparation). Our results and those of a recent report on the *LMNA* locus[31] indicate that, as in the case of ZFN-mediated HR, HDAdV-mediated HR is not affected by the transcriptional activities of the target chromosomal loci. The efficiencies of accurate gene targeting varied depending on the target locus and the cell line but remained consistently high. In this study, to determine the accuracy of HR, the candidate targeted clones were screened by PCR, followed by Southern analyses. Long homology arms hamper detailed Southern analyses to examine the accuracy of HR by BAC-mediated methods. Additional ectopic integrations have been observed in ZFN-mediated targeted hES and hiPS clones.[10] HDAdVs yielded 3–55% of chromosomal integration of the vectors ($G418^R$ colonies) at the target loci, based on PCR analyses (**Table 1**). These numbers indicate strong affinity of gene-targeting cassettes delivered by HDAdVs with homologous chromosomal sequences even without artificial DNA DSBs. Detailed Southern analyses with multiple probes and enzymes confirmed that 75–100% of these site-specific integration events were mediated by accurate HR (**Supplementary Figure S1**). Similar detailed analyses of the structure of integrated gene-targeting cassettes delivered by electroporation into the *HPRT* locus in mouse ES cells reveal that only 5% of $6TG^R$ colonies are generated by accurate HR,[32] indicating high fidelity of HDAdV-mediated gene targeting. Overall, the relative gene-targeting efficiencies were 3–55% and 7–81% of $G418^R$ colonies and $G418^R$/$GANC^R$ colonies, respectively. Furthermore, gene targeting was equally efficient even at a transcriptionally silent target. Although the cells were maintained under drug (G418 and GANC) selection, deleterious effects were not observed, at least by the analyses of the karyotype, pluripotency, and growth rates of the cells (**Figure 5**, **Supplementary Figure S2**, and data not shown). More data from other loci will be needed to elucidate why the gene-targeting efficiency is particularly high at the *KU80* locus. Importantly, in contrast to ZFN-mediated gene targeting, no additional ectopic chromosomal integrations of the vectors were detected in any of the 47 HDAdV-mediated homologous recombinants (**Table 1**). Inaccurate homologous recombinants (**Figure 3c,d**) might have been produced by the mechanism described by Adair *et al.*[33] The absolute gene-targeting frequencies with HDAdVs were 2.0×10^{-7} to 5.6×10^{-5} per infected cell (9.0×10^{-6} on average). Therefore, depending on the target locus, the absolute efficiency with HDAdVs is as high as that obtained by using ZFNs (see above). This also indicates that a 100-mm dish of starting hiPSCs (~3×10^6 cells) is sufficient to obtain multiple gene-targeted clones. Furthermore, in contrast to

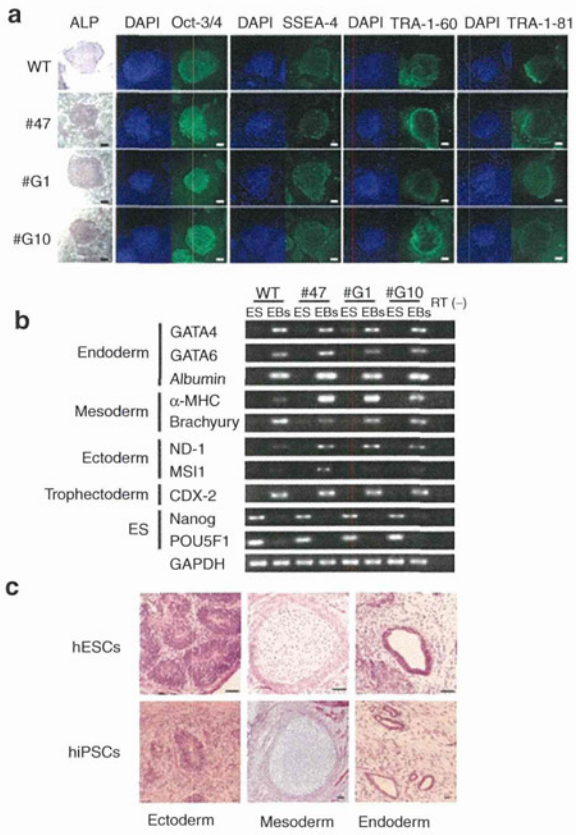

Figure 5 Characterization of *HB9*-EGFP knock-in hESC and hiPSC clones. (**a**) Expression of stem cell markers in the *HB9*-EGFP knock-in hESC clones (#47, #G1, and #G10). ALP, alkaline phosphatase. Bars, 200 mm. (**b**) Multipotency of the *HB9*-EGFP knock-in hESC clones. Embryoid bodies (EBs) derived from the hESCs were analyzed by RT-PCR for expression of the lineage-specific markers. *GAPDH* was used as a control. RT (–), without reverse transcriptase. (**c**) *In vivo* differentiation of *HB9*-EGFP knock-in hESC (#47) and hiPSC (#24) clones. Tissues derived from three germ layers are indicated. Bars, 50 mm. EGFP, enhanced green fluorescent protein; hESC, human embryonic stem cell; hiPSC, human induced pluripotent stem cell; RT-PCR, reverse transcription.

electroporation, which requires ten million cells for each attempt, HDAdV-mediated gene targeting is equally efficient even with a smaller number of starting cells,[34] which minimizes the number of passages/cell divisions to obtain homologous recombinants.

HR has to be accurate for applications such as establishment of gene knock-in iPSC lines to obtain tissue-specific expression of an inserted marker gene upon differentiation. Furthermore, unintended mutations during chromosomal manipulation are obviously not acceptable for therapeutic applications of hESCs/hiPSCs. The characteristics of highly efficient gene-targeting strategies indicate that BAC-mediated gene targeting might be useful for making heterozygote mutants at housekeeping loci because the procedure is relatively simple. ZFN-mediated gene targeting would be useful for making marker gene knock-ins or homozygous mutants because of its relatively high absolute targeting efficiency. Finally, HDAdVs would be the best suited for manipulation of iPSCs for clinical applications, such as gene repair therapy of inherited disorders, because of the highly efficient and accurate gene targeting with minimal cytotoxicity at both transcriptionally active and inactive loci.

MATERIALS AND METHODS

Construction and preparation of HDAdVs. The human *HPRT1*-targeting HDAdV was described previously.[16] To construct the human *HB9*-EGFP knock-in HDAdV, 5′ and 3′ homologous arms were amplified from KhES-1 genomic DNA by PCR. The ATG start codon of EGFP gene was fused in-frame with the ATG of *HB9* gene. The fragments were then introduced into the pBluescriptII-based vector plasmid encoding the PGK-neo-pA cassette which was sandwiched by *lox*P sites and then the whole targeting cassette was subcloned into an HDAdV plasmid. To generate the human *KU80, LIG1*, and *LIG3* gene-targeting vectors, BAC clones containing the human *KU80, LIG1*, and *LIG3* loci (BACPAC resources, Oakland, CA) were modified by using the RED/ET recombination technique.[35] The *lox*P71-PGK-EM7-neo-bpA-*lox*P66 cassette was inserted into the target sites on these BAC clones (**Figures 2a** and **3a,b**). Subsequently, a total of 22–23 kb of homologies including the marker cassette was subcloned into the HDAdV plasmid. A detailed description of these subclonings will be provided on request. The HDAdVs were propagated by serial passages on 293FLPe with addition of FL helper virus (kindly provided by Pedro Lowenstein)[36] and purified, as described previously.[37] Vector genome titers were determined by quantitative Southern analyses.

Culture of hESCs and hiPSCs. hESC lines, KhES-1 subline 1 and KhES-3,[38,39] and hiPSC lines, 246H1 and 246G1 (kindly provided by Shinya Yamanaka),[17] were maintained, as previously described.[39] 246H1 was derived from neonate fibroblast BJ cells with three factors (OCT3/4, SOX2, and KLF4). The hESC lines were used following the hESC research guidelines of the Japanese government.

Isolation of the gene-targeted clones. Clumps of hESCs and hiPSCs were infected with the HDAdVs at a multiplicity of infection of 1,000 vector genomes/cell. Electroporation of plasmid DNA was performed, as reported previously.[3] G418 selection (50 μg/ml; Nacalai tesque, Kyoto, Japan) was started 2 days after infection or electroporation. After 3 weeks, surviving colonies were transferred to 96-well plates and GANC selection (2 μmol/l; Invitrogen, Carlsbad, CA) was started. For gene targeting at *HRPT1*, 6TG (10 mmol/l; Sigma-Aldrich, St Louis, MO) selection was applied after the G418 selection and the 6TG-resistant clones were analyzed. For other loci, G418/GANC double-resistant clones were characterized. Genomic DNA of drug-resistant clones was subject to screening by PCR using primers shown in **Table 2** with LA Taq Hot Start Version (TAKARA, Kyoto, Japan) or PrimeSTAR GXL polymerase (TAKARA), following the manufacturer's protocol. To analyze the structure of *HB9*, *KU80*, *LIG1*, and *LIG3* loci, DNA was extracted from PCR-positive clones. The accuracy of gene targeting was carefully evaluated by the Southern analyses using restriction enzyme(s), which digested outside the homology arms and also inside the marker gene cassettes, but not within the homology arms. The 5′ and 3′ probes were located between the homology arms and the restriction enzyme sites. Restriction enzymes and probes for Southern hybridization are indicated in **Figures 1a, 2a, 3a,b,** and **4a**. Additional ectopic integration of the vector is therefore expected to produce an extra band with the neo or GFP probe.

For the chromosomal analyses, gene knockout and knock-in hES clones were treated with 100 ng/ml colcemid (Invitrogen) for 2 hours, trypsinized, incubated in 0.075 mol/l KCl for 14 minutes, and fixed in Carnoy's fixative. The cells were spread onto glass slides and stained with Giemsa. Chromosome spreads were analyzed by randomly counting 50 cells using the Ikaros Karyotyping System (MetaSystems, Waltham, MA).

Excision of the neomycin-resistant gene cassette in targeted clones. Clumps of hiPSCs were plated feeder-free and transfected with a pCAGGS-Cre plasmid, the CAG promoter-driven Cre gene, using FuGENE HD (Roche, Basel, Switzerland), according to the manufacturer's instructions. Six days later, the cells were sorted into single cells in the presence of Rho-associated coiled kinase (ROCK) inhibitor Y-27632 (10 μmol/l; Wako,

Table 2 Primer sequences used in this study

Gene		Sequence (5′ to 3′)
Screening of the drug-resistant clone		
HB9	5′ KO primer set	TGCGACTGTGTCCTGATGCCCGACTGTAAGCTG
		CGATGTTGTGGCGGATCTTGAAGTTCACCTTGA
	3′ KO primer set	TCTTGTCGATCAGGATGATCTGGACGAAGAG
		GGAGGACTTCTCAGAACACATTCCGCCGTCTTTG
KU80	5′ KO primer set	CTCAGAAAGCACAGAACTAGGCATGAGAAG
		CTCTTCGTCCAGATCATCCTGATCGACAAGA
	3′ KO primer set	TCTTGTCGATCAGGATGATCTGGACGAAGAG
		GGAGGCTTATATGAAGGCACGCATCAGATTCCTAC
LIG1	5′ KO primer set	AGGGATGAGAGGGCGGATGAAGGCATGAAT
		CTCTTCGTCCAGATCATCCTGATCGACAAGA
	3′ KO primer set	TCTTGTCGATCAGGATGATCTGGACGAAGAG
		TTCTATCTTGTGCCAATCCAATGTGCCTGTAAAGC
LIG3	5′ KO primer set	CAAAAACGCACTTTACTCTCCACCCTAACTAGCTGA
		CTCTTCGTCCAGATCATCCTGATCGACAAGA
	3′ KO primer set	TCTTGTCGATCAGGATGATCTGGACGAAGAG
		CTGGGAGAACAAGATTATGTGTCCATCTGCTGTGA
Albumin for RT-PCR		GTTGCTCATCGGTTTAAAGATTTGGGAGAAGAA
		AGGTTTGGGTTGTCATCTTTGTGTTGCAAG
Telomere-specific primer		TTAGGGTTAGGGTTAGGGTTAGGG

RT-PCR, reverse transcription-PCR.

Osaka, Japan) onto 96-well plates by using FACS Aria II (BD, Franklin Lakes, NJ). The removal of the *neo* cassette was confirmed by G418 sensitivity, PCR, and Southern hybridization, and the surviving colonies were used for motor neuron differentiation.

Motor neuron differentiation. Motor neuron induction was performed, as previously described with some modifications.[40] Briefly, dissociated iPSC colonies were plated onto culture dishes coated with poly-L-lysine/laminin (PLL/LM; Sigma-Aldrich) in N2B27 neural differentiation medium (1:1 mix of Dulbecco's modified Eagle medium/F12 supplemented with N2 and neurobasal medium supplemented with B27, all from Life Technologies, Carlsbad, CA), supplemented with mouse recombinant Noggin (100 ng/ml; R&D Systems, Minneapolis, MN) for 10 days. Subsequently, colonies were split into small clumps by treatment with Collagenase (200 U/ml; Life Technologies) with 1 mmol/l $CaCl_2$ and cultured on new poly-L-lysine/laminin-coated dishes with N2B27 supplemented with Noggin for 7 additional days. The cells were, then, dissociated by Accutase (Innovative Cell Technologies, San Diego, CA) and cultured on dishes coated with poly-L-lysine/laminin plus human plasma Fibronectin (PL/LM/FN) (Chemicon, Billerica, MA) in N2B27 supplemented with 1 µmol/l of retinoic acid (RA; Sigma-Aldrich) for 4 days, and then cultured in N2B27 supplemented with retinoic acid and human recombinant sonic hedgehog (500 nmol/l; R&D Systems) for additional 7–9 days. The cells were again dissociated by Accutase and cultured on poly-L-lysine/laminin plus human plasma Fibronectin-coated dishes in N2B27 supplemented with brain-derived neurotrophic factor (10 ng/ml; R&D Systems), glial cell-derived neurotrophic factor (10 ng/ml; R&D Systems), and neurotrophin-3 (10 ng/ml; R&D Systems) for another 5 days. Finally, the cells were fixed with 4% paraformaldehyde and subjected to direct visualization of EGFP and immunocytochemistry of HB9 protein, as previously described.[40]

Quantitative RT-PCR assay and western blot assay. RNA extraction and cDNA synthesis for quantitative RT-PCR were carried out as previously described.[16] The ABI PRISM 7000 sequence detection system (Applied Biosystems, Carlsbad, CA) was used for quantitative RT-PCR. Predesigned primers and probe sets for *KU80* (Hs00221707_m1), *LIG1* (Hs01553527_m1), *LIG3* (Hs00242692_m1), and *GAPDH* (Hs99999905_m1) were obtained from Applied Biosystems. Western blot assays were performed with anti-*KU80* (C-20; Santa Cruz Biotechnology, Santa Cruz, CA), anti-*LIG1* (10H5; Abcam, Cambridge, MA), anti-*LIG3* (1F3; Abcam), or anti-α-tubulin (DM1A; Santa Cruz Biotechnology) antibodies. The membranes were subsequently probed with a horseradish peroxidase-conjugated secondary antibody (anti-goat IgG-HRP or anti-mouse IgG-HRP; Santa Cruz Biotechnology) and developed with ECL PLUS (GE Healthcare, Piscataway, NJ).

Analyses of the stem cell markers and pluripotency. Expression of alkaline phosphatase and surface markers, such as SSEA-4, TRA-1-60, and TRA-1-81, was examined, as previously described.[16] Formation of embryoid bodies, RNA extraction, and cDNA synthesis were previously described.[16] The sequence of *Albumin*-specific primers are shown in Table 2. The sequences of other primers were previously described.[16] Formation of teratoma and hematoxylin and eosin staining were performed with *HB9*-EGFP knock-in hESC and hiPSC clones, as previously described.[39] Animal protocols were approved by the Institutional Board on Animal Care.

SUPPLEMENTARY MATERIAL

Figure S1. Examples of Southern analyses.
Figure S2. Karyotype analyses.
Figure S3. Motor neurons differentiated from the *HB-9*-EGFP knock-in hESC clone.
Table S1. The number of colonies in which the selection marker was excised.

ACKNOWLEDGMENTS

We thank the members of Mitani lab, Haruyoshi Takaki (Teikyo University) and Mizuki Ohno (Kyushu University), for helpful discussions, Ayako Tokumitsu (Saitama Medical University) for technical supports, Tomoaki Hishida (Saitama Medical University) for advice on quantitative RT-PCR and western blotting, Pedro R. Lowenstein (Cedars-Sinai Medical Center) for providing 293FLPe cells and FL helper virus, and Shinya Yamanaka (Kyoto University) for providing human iPSC lines (246G1 and 246H1). This work was supported by national funds from Development of Technology to Create Research Model Cells Project of New Energy and Industrial Technology Development Organization (NEDO) to N.N. and K.M. and, in part, by a grant-in-aid for "Support Project of Strategic Research Center in Private Universities" from the Ministry of Education, Culture, Sports, Science and Technology (MEXT) to Research Center for Genomic Medicine, Saitama Medical University. The authors declare no conflict of interest.

REFERENCES

1. Nieminen, M, Tuuri, T and Savilahti, H (2010). Genetic recombination pathways and their application for genome modification of human embryonic stem cells. *Exp Cell Res* **316**: 2578–2586.
2. Tenzen, T, Zembowicz, F and Cowan, CA (2010). Genome modification in human embryonic stem cells. *J Cell Physiol* **222**: 278–281.
3. Zwaka, TP and Thomson, JA (2003). Homologous recombination in human embryonic stem cells. *Nat Biotechnol* **21**: 319–321.
4. Urbach, A, Schuldiner, M and Benvenisty, N (2004). Modeling for Lesch-Nyhan disease by gene targeting in human embryonic stem cells. *Stem Cells* **22**: 635–641.
5. Di Domenico, AI, Christodoulou, I, Pells, SC, McWhir, J and Thomson, AJ (2008). Sequential genetic modification of the hprt locus in human ESCs combining gene targeting and recombinase-mediated cassette exchange. *Cloning Stem Cells* **10**: 217–230.
6. Ruby, KM and Zheng, B (2009). Gene targeting in a HUES line of human embryonic stem cells via electroporation. *Stem Cells* **27**: 1496–1506.
7. Sakurai, K, Shimoji, M, Tahimic, CG, Aiba, K, Kawase, E, Hasegawa, K *et al.* (2010). Efficient integration of transgenes into a defined locus in human embryonic stem cells. *Nucleic Acids Res* **38**: e96.
8. Song, H, Chung, SK and Xu, Y (2010). Modeling disease in human ESCs using an efficient BAC-based homologous recombination system. *Cell Stem Cell* **6**: 80–89.
9. Lombardo, A, Genovese, P, Beausejour, CM, Colleoni, S, Lee, YL, Kim, KA *et al.* (2007). Gene editing in human stem cells using zinc finger nucleases and integrase-defective lentiviral vector delivery. *Nat Biotechnol* **25**: 1298–1306.
10. Hockemeyer, D, Soldner, F, Beard, C, Gao, Q, Mitalipova, M, DeKelver, RC *et al.* (2009). Efficient targeting of expressed and silent genes in human ESCs and iPSCs using zinc-finger nucleases. *Nat Biotechnol* **27**: 851–857.
11. Zou, J, Maeder, ML, Mali, P, Pruett-Miller, SM, Thibodeau-Beganny, S, Chou, BK *et al.* (2009). Gene targeting of a disease-related gene in human induced pluripotent stem and embryonic stem cells. *Cell Stem Cell* **5**: 97–110.
12. Mitsui, K, Suzuki, K, Aizawa, E, Kawase, E, Suemori, H, Nakatsuji, N *et al.* (2009). Gene targeting in human pluripotent stem cells with adeno-associated virus vectors. *Biochem Biophys Res Commun* **388**: 711–717.
13. Khan, IF, Hirata, RK, Wang, PR, Li, Y, Kho, J, Nelson, A *et al.* (2010). Engineering of human pluripotent stem cells by AAV-mediated gene targeting. *Mol Ther* **18**: 1192–1199.
14. Mitani, K, Graham, FL, Caskey, CT and Kochanek, S (1995). Rescue, propagation, and partial purification of a helper virus-dependent adenovirus vector. *Proc Natl Acad Sci USA* **92**: 3854–3858.
15. Palmer, DJ and Ng, P (2005). Helper-dependent adenoviral vectors for gene therapy. *Hum Gene Ther* **16**: 1–16.
16. Suzuki, K, Mitsui, K, Aizawa, E, Hasegawa, K, Kawase, E, Yamagishi, T *et al.* (2008). Highly efficient transient gene expression and gene targeting in primate embryonic stem cells with helper-dependent adenoviral vectors. *Proc Natl Acad Sci USA* **105**: 13781–13786.
17. Takahashi, K, Tanabe, K, Ohnuki, M, Narita, M, Ichisaka, T, Tomoda, K *et al.* (2007). Induction of pluripotent stem cells from adult human fibroblasts by defined factors. *Cell* **131**: 861–872.
18. Bertolini, LR, Bertolini, M, Maga, EA, Madden, KR and Murray, JD (2009). Increased gene targeting in Ku70 and Xrcc4 transiently deficient human somatic cells. *Mol Biotechnol* **41**: 106–114.
19. Fattah, FJ, Lichter, NF, Fattah, KR, Oh, S and Hendrickson, EA (2008). Ku70, an essential gene, modulates the frequency of rAAV-mediated gene targeting in human somatic cells. *Proc Natl Acad Sci USA* **105**: 8703–8708.
20. Harrison, KA, Druey, KM, Deguchi, Y, Tuscano, JM and Kehrl, JH (1994). A novel human homeobox gene distantly related to proboscipedia is expressed in lymphoid and pancreatic tissues. *J Biol Chem* **269**: 19968–19975.
21. Arber, S, Han, B, Mendelsohn, M, Smith, M, Jessell, TM and Sockanathan, S (1999). Requirement for the homeobox gene Hb9 in the consolidation of motor neuron identity. *Neuron* **23**: 659–674.
22. Thaler, J, Harrison, K, Sharma, K, Lettieri, K, Kehrl, J and Pfaff, SL (1999). Active suppression of interneuron programs within developing motor neurons revealed by analysis of homeodomain factor HB9. *Neuron* **23**: 675–687.
23. Durai, S, Mani, M, Kandavelou, K, Wu, J, Porteus, MH and Chandrasegaran, S (2005). Zinc finger nucleases: custom-designed molecular scissors for genome engineering of plant and mammalian cells. *Nucleic Acids Res* **33**: 5978–5990.
24. Porteus, MH and Carroll, D (2005). Gene targeting using zinc finger nucleases. *Nat Biotechnol* **23**: 967–973.
25. Händel, EM and Cathomen, T (2011). Zinc-finger nuclease based genome surgery: it's all about specificity. *Curr Gene Ther* **11**: 28–37.
26. Gupta, A, Meng, X, Zhu, LJ, Lawson, ND and Wolfe, SA (2011). Zinc finger protein-dependent and -independent contributions to the *in vivo* off-target activity of zinc finger nucleases. *Nucleic Acids Res* **39**: 381–392.
27. Olsen, PA, Gelazauskaite, M, Randøl, M and Krauss, S (2010). Analysis of illegitimate genomic integration mediated by zinc-finger nucleases: implications for specificity of targeted gene correction. *BMC Mol Biol* **11**: 35.
28. Radecke, S, Radecke, F, Cathomen, T and Schwarz, K (2010). Zinc-finger nuclease-induced gene repair with oligodeoxynucleotides: wanted and unwanted target locus modifications. *Mol Ther* **18**: 743–753.
29. Khan, IF, Hirata, RK and Russell, DW (2011). AAV-mediated gene targeting methods for human cells. *Nat Protoc* **6**: 482–501.
30. Aarts, M and te Riele, H (2011). Progress and prospects: oligonucleotide-directed gene modification in mouse embryonic stem cells: a route to therapeutic application. *Gene Ther* **18**: 213–219.
31. Liu, GH, Suzuki, K, Qu, J, Sancho-Martinez, I, Yi, F, Li, M *et al.* (2011). Targeted gene correction of laminopathy-associated LMNA mutations in patient-specific iPSCs. *Cell Stem Cell* **8**: 688–694.
32. Hasty, P, Rivera-Pérez, J, Chang, C and Bradley, A (1991). Target frequency and integration pattern for insertion and replacement vectors in embryonic stem cells. *Mol Cell Biol* **11**: 4509–4517.
33. Adair, GM, Nairn, RS, Wilson, JH, Seidman, MM, Brotherman, KA, MacKinnon, C *et al.* (1989). Targeted homologous recombination at the endogenous adenine phosphoribosyltransferase locus in Chinese hamster cells. *Proc Natl Acad Sci USA* **86**: 4574–4578.
34. Ohbayashi, F, Balamotis, MA, Kishimoto, A, Aizawa, E, Diaz, A, Hasty, P *et al.* (2005). Correction of chromosomal mutation and random integration in embryonic stem cells with helper-dependent adenoviral vectors. *Proc Natl Acad Sci USA* **102**: 13628–13633.
35. Datsenko, KA and Wanner, BL (2000). One-step inactivation of chromosomal genes in Escherichia coli K-12 using PCR products. *Proc Natl Acad Sci USA* **97**: 6640–6645.
36. Umaña, P, Gerdes, CA, Stone, D, Davis, JR, Ward, D, Castro, MG *et al.* (2001). Efficient FLPe recombinase enables scalable production of helper-dependent adenoviral vectors with negligible helper-virus contamination. *Nat Biotechnol* **19**: 582–585.
37. Palmer, DJ and Ng, P (2004). Physical and infectious titers of helper-dependent adenoviral vectors: a method of direct comparison to the adenovirus reference material. *Mol Ther* **10**: 792–798.
38. Hasegawa, K, Fujioka, T, Nakamura, Y, Nakatsuji, N and Suemori, H (2006). A method for the selection of human embryonic stem cell sublines with high replating efficiency after single-cell dissociation. *Stem Cells* **24**: 2649–2660.
39. Suemori, H, Yasuchika, K, Hasegawa, K, Fujioka, T, Tsuneyoshi, N and Nakatsuji, N (2006). Efficient establishment of human embryonic stem cell lines and long-term maintenance with stable karyotype by enzymatic bulk passage. *Biochem Biophys Res Commun* **345**: 926–932.
40. Wada, T, Honda, M, Minami, I, Tooi, N, Amagai, Y, Nakatsuji, N *et al.* (2009). Highly efficient differentiation and enrichment of spinal motor neurons derived from human and monkey embryonic stem cells. *PLoS ONE* **4**: e6722.
41. Nagai, T, Ibata, K, Park, ES, Kubota, M, Mikoshiba, K and Miyawaki, A (2002). A variant of yellow fluorescent protein with fast and efficient maturation for cell-biological applications. *Nat Biotechnol* **20**: 87–90.